BJ www.biochemj.org

Biochem. J. (2012) **441**, 487–498 (Printed in Great Britain) doi:10.1042/BJ20111199

online data

Directed evolution of a temperature-, peroxide- and alkaline pH-tolerant versatile peroxidase

Eva GARCIA-RUIZ*, David GONZALEZ-PEREZ*, Francisco J. RUIZ-DUEÑAS†, Angel T. MARTÍNEZ† and Miguel ALCALDE*[1]

*Department of Biocatalysis, Institute of Catalysis, CSIC, Cantoblanco, 28049 Madrid, Spain, and †Center for Biological Investigations, CSIC, Ramiro de Maeztu 9, 28040 Madrid, Spain

The VPs (versatile peroxidases) secreted by white-rot fungi are involved in the natural decay of lignin. In the present study, a fusion gene containing the VP from *Pleurotus eryngii* was subjected to six rounds of directed evolution, achieving a level of secretion in *Saccharomyces cerevisiae* (21 mg/l) as yet unseen for any ligninolytic peroxidase. The evolved variant for expression harboured four mutations and increased its total VP activity 129-fold. The signal leader processing by the *STE13* protease at the Golgi compartment changed as a consequence of overexpression, retaining the additional N-terminal sequence Glu-Ala-Glu-Ala that enhanced secretion. The engineered N-terminally truncated variant displayed similar biochemical properties to those of the non-truncated counterpart in terms of kinetics, stability and spectroscopic features. Additional cycles of evolution raised the T_{50} 8 °C and significantly increased the enzyme's stability at alkaline pHs. In addition, the K_m for H_2O_2 was enhanced up to 15-fold while the catalytic efficiency was maintained, and there was an improvement in peroxide stability (with half-lives for H_2O_2 of 43 min at a H_2O_2/enzyme molar ratio of 4000:1). Overall, the directed evolution approach described provides a set of strategies for selecting VPs with improvements in secretion, activity and stability.

Key words: α-factor prepro-leader, directed evolution, enzyme promiscuity, *Saccharomyces cerevisiae*, versatile peroxidase.

INTRODUCTION

The ligninolytic enzymatic consortium secreted by white-rot fungi represents a remarkable example of a highly efficient oxidative system [1]. For decades, the complex interactions and synergies between enzymes and diffusible electron carriers generated by the wood-decaying fungi during lignin combustion have constituted a hot topic of research [2]. Typically formed by different oxidoreductases (mostly laccases, peroxidases and H_2O_2-supplying oxidases), this lignin-degrading array of enzymes have potential applications in the production of second-generation biofuels, pulp biobleaching, the design of nanobiodevices (biosensors and biofuel cells), organic synthesis and bioremediation, to name a few [3–6]. Among these enzymes, the high-redox potential VP (versatile peroxidase) is arousing great interest because of its catalytic promiscuity, being mainly described in *Pleurotus*, *Bjerkandera* and some other basidiomycete species [7–13].

As a protein, VP is classified by its structural properties and sequence information in Class II, corresponding to fungal secreted haem-containing peroxidases. As an enzyme, it is presented as a high-redox-potential substrate and Mn^{2+}-oxidizing peroxidase (E.C. 1.11.1.6) [14]. VPs combine the general catalytic features of other haem-containing enzymes (in terms of substrate specificity and reaction mechanisms), such as the high-redox-potential ligninolytic peroxidases, LiP (lignin peroxidase) and MnP (manganese peroxidase), with those of peroxidases with a lower redox potential, such as HRP (horseradish peroxidase) and CIP (*Coprinopsis cinerea* peroxidase) [15]. The VP's substrate promiscuity is associated with a high redox potential ($E^\circ > +1.4$ V) and the presence of different catalytic sites for the oxidation of low- and high-redox-potential compounds [14,16]. Comprehensive structure–function studies have helped to reveal the mechanisms underlying the complex activity of these enzymes, which is governed by a haem domain located in the middle of a structure formed by 12 helices and that is connected to the protein surface by two small channels. In a scaffold of ~300 amino acids, VPs contain three carboxy residues implicated in the co-ordination of Mn^{2+} and one catalytic tryptophan residue involved in the oxidation of high-redox-potential compounds through a long-range electron-transfer pathway. In addition, VP has an oxidation site for low–medium-redox-potential compounds (0.6–0.8 V) associated with the main haem-access channel [17–19]. Thus VP behaves as a generalist biocatalyst, readily oxidizing VA (veratryl alcohol), methoxybenzenes or non-phenolic lignin model compounds (such as LiP); Mn^{2+} to Mn^{3+} (such as MnP), the latter able to act as diffusible oxidizer; and phenolic compounds (such as HRP and CIP). Furthermore, and unlike laccases that require the help of redox mediators [20], VPs can oxidize high-redox-potential compounds alone, such as polycyclic aromatic hydrocarbons, azo-dyes and many other complex recalcitrant molecules that LiP only oxidizes in the presence of VA [16].

Despite its broad catalytic promiscuity, the lack of a suitable heterologous host to functionally express VPs has impeded their engineering by directed evolution. Their extreme structural complexity (four disulfide bridges, two structural Ca^{2+}, the haem prosthetic group) often hampers proper folding and functional expression at reasonable levels. Indeed, when *Emericella nidulans*

Abbreviations used: ABTS, 2,2′-azinobis-(3-ethylbenzothiazoline-6-sulfonic acid); CIP, *Coprinopsis cinerea* peroxidase; DMP, 2,6-dimethoxyphenol; HRP, horseradish peroxidase; IvAM, *in vivo* assembly of mutant libraries constructed with different mutational spectra; IVOE, *in vivo* overlap extension; LiP, lignin peroxidase; MALDI–TOF-MS, matrix-assisted laser-desorption ionization–time-of-flight MS; MnP, manganese peroxidase; RB5, Reactive Black 5; StEP, staggered extension process; TAI, total activity improvement; VA, veratryl alcohol; VP, versatile peroxidase.

[1] To whom correspondence should be addressed (email malcalde@icp.csic.es).

or *Aspergillus niger* have been tested as hosts, VP expression was similar to that achieved from the homologous VP in *Pleurotus eryngii* (~0.4 mg/l) [21]. Moreover, further optimization by engineering only slightly improved the yields of secretion up to 2 mg/l [22,23]. When *Escherichia coli* has been used (one of the favourite hosts for directed evolution along with *Saccharomyces cerevisiae*), inclusion bodies were generally formed, and when a soluble enzyme was obtained, its atypical properties were related to improper folding [24]. In *E. coli*, the *in vitro* refolding from inclusion bodies can be attempted [25], which, although useful for structure–function studies [17–19], is not appropriate for high-throughput screening or directed evolution experiments. Rather than facing the shortcomings found for correct VP folding in bacteria (from different codon usage to the lack of post-translational modifications and missing chaperones), we circumvented these bottlenecks by engineering strategies to perform laboratory evolution of VP in *S. cerevisiae*. In the present paper, we report for the first time an evolved VP produced heterologously and functionally in a soluble, active and stable form. To extract further benefits from this system, additional rounds of molecular evolution were carried out to tailor a highly stable enzyme. The laboratory evolution approach based on the yeast eukaryotic machinery is discussed in detail, together with the properties of a set of novel VPs that include strong functional expression and improved stability against temperature, alkaline pH and inactivation by H_2O_2. A comprehensive biochemical analysis of the VP variants is provided.

EXPERIMENTAL

Laboratory evolution: general aspects

The original parental *α-vpl2* fusion gene was constructed as described in the Supplementary Experimental section at http://www.BiochemJ.org/bj/441/bj4410487add.htm. In each generation, PCR fragments were cleaned, concentrated and loaded on to a low-melting-point preparative agarose gel for purification using the Zymoclean gel DNA recovery kit (Zymo Research). PCR products were cloned under the control of GAL1p in the pJRoC30 expression shuttle vector, replacing the native gene in pJRoC30. The pJRoC30 plasmid was linearized with XhoI and BamHI to remove the native gene, and the linear plasmid was concentrated and purified as described above for the PCR fragments.

Evolution for secretion: first generation

A mutagenic library (~1400 clones) was constructed by error-prone PCR using the following primers for amplification: RMLN sense primer, 5′-CCTCTATACTTTAACGTCAAGG-3′, which binds to bp 160–181 of pJRoC30-*αvpl2*; and RMLC antisense primer, 5′-GGGAGGGCGTGAATGTAAGC-3′, which binds to bp 1532–1551 of pJRoC30-*αvpl2*. To promote *in vivo* ligation, overhangs of 40 and 66 bp homologous with the linear vector were designed. The reaction mixture was prepared in a final volume of 50 μl containing 90 nM RMLN primer, 90 nM RMLC primer, 0.1 ng/μl pJRoC30-*αvpl2*, 0.3 mM dNTPs (0.075 mM each), 3 % DMSO, 1.5 mM $MgCl_2$ and 0.05 unit/μl Taq DNA polymerase (Sigma). Different concentrations of $MnCl_2$ were tested to estimate the appropriate mutation rate before adopting 0.01 mM as the final concentration. Error-prone PCR was carried out on a gradient thermocycler (MyCycler, Bio-Rad Laboratories) using the following programme: 95 °C for 2 min (1 cycle); 94 °C for 0.45 min, 53 °C for 0.45 min, 74 °C for 3 min (28 cycles); and 74 °C for 10 min (1 cycle).The PCR product (400 ng) was mixed with the linearized vector (100 ng) and transformed into competent cells using the yeast transformation kit (Sigma). Transformed cells were plated in SC (synthetic complete) drop-out plates and incubated for 3 days at 30 °C. Colonies containing the whole autonomously replicating vector were picked and screened, and then subjected to additional screenings as described in the Supplementary Experimental section. From the first to the fourth round of evolution, the libraries were explored for improvements in total activity. From the fourth round onwards, libraries were explored for improvements in thermostability. Here and in other parts of the study, VP activity was measured by oxidation of 2 mM ABTS [2,2′-azinobis-(3-ethylbenzothiazoline-6-sulfonic acid)] ($\varepsilon_{ABTS^{\bullet+}} = 36000\ M^{-1} \cdot cm^{-1}$) in 100 mM sodium tartrate buffer, pH 3.5 (the optimum ABTS oxidation value for the VPL2 parent) in the presence of 0.1 mM H_2O_2.

Evolution for secretion: second generation

The best secretion variants from the first round (11H10, 15G9, 4B5 and 4B1; Figure 1) were subjected to Taq/$MnCl_2$ amplification and recombined further by *in vivo* DNA shuffling (~1800 clones). The Taq/$MnCl_2$ amplifications were prepared as described above for the first round. Mutated PCR products were mixed in equimolar amounts and transformed along with the linearized vector into yeast (4:1 ratio of PCR products/vector).

Evolution for secretion: third generation

The best secretion variants of the second round (16E12, 19C2, 20D1 and 13G1; Figure 1) were subjected to Taq/$MnCl_2$ amplification and recombined by *in vivo* DNA shuffling (~1100 clones) as described for the second generation.

Evolution for secretion and thermostability: fourth generation

The best secretion variants of the third round (10C3, 6B1, 13E4, 6E7 and 11F3; Figure 1) were subjected to mutagenic StEP (staggered extension process) and *in vivo* DNA shuffling (~2000 clones). StEP was performed as reported previously [26] with some modifications. In order to favour random mutagenesis during StEP, Taq DNA polymerase was employed for the PCR reaction along with a low template concentration to promote the introduction of point mutations during amplification. The PCRs were performed in a final volume of 50 μl containing 90 nM RMLN primer, 90 nM RMLC primer, 0.3 mM dNTPs, 3 % DMSO, 0.05 unit/μl of Taq polymerase (Sigma), 1.5 mM $MgCl_2$ and 0.1 ng/μl of the 10C3, 6B1, 13E4, 6E7 and 11F3 DNA-template mixture. The thermal cycling programme for StEP was: 95 °C for 5 min (1 cycle), and 94 °C for 30 s and 55 °C for 20 s (90 cycles). Purified PCR products were recombined further by *in vivo* DNA shuffling as described for earlier generations. A thermostability assay was incorporated to screen this and future generations (see the Supplementary Experimental section for details). The temperature established to screen this generation was 60 °C.

Evolution for thermostability: fifth generation

A library of ~1400 clones was built by IvAM (*in vivo* assembly of mutant libraries constructed with different mutational spectra) [27]. The 24E10 thermostable mutant was used as the parental type (Figure 1), and Taq/$MnCl_2$ (Sigma) and Mutazyme libraries (Stratagene) were mixed in equimolar amounts, and they were transformed into competent *S. cerevisiae* cells along with the linearized vector as described above (4:1 ratio of

library/vector). The library was explored by thermostability screening as described in the Supplementary Experimental section. The temperature established to screen this generation was 80 °C.

Evolution for thermostability: sixth generation

The best thermostable variants of the former round (3H9 and 15B4; Figure 1) were subjected to Taq/$MnCl_2$ amplification and recombined by *in vivo* DNA shuffling (~1400 clones) as described for the third generation. The library was screened as described for the previous generation with the screening temperature established as 90 °C.

Engineering truncated variants

In order to remove the extra N-terminal sequence, the best secretion mutant (R4, fourth generation) was subjected to deletion mutagenesis by IVOE (*in vivo* overlap extension) [28] (see details in the Supplementary Experimental section).

High-throughput screening

Activity and thermostability screening assays were performed as indicated in the Supplementary Experimental section. Selected mutants were produced, purified and characterized as described in the Supplementary Experimental section.

RESULTS AND DISCUSSION

Directed evolution strategy

Our starting point in the present study was the cDNA of the high-redox potential VP from the white-rot fungus *P. eryngii* (allelic variant *vpl2*). This gene encodes a mature protein of 331 amino acids, with a 30-amino-acid signal leader that directs its secretion. Initially, the native VP signal leader was replaced by the α-factor prepro-leader from *S. cerevisiae*, a commonly used signal peptide for heterologous protein expression in yeast [29]. The fusion gene constructed (*α-vpl2*) was cloned into the corresponding shuttle vector and was shown to be functionally expressed in *S. cerevisiae* (120 ABTS units/l of culture flask). The medium composition (haem supply, ethanol content and $CaCl_2$ content) and the culture conditions (temperature, pH, oxygen uptake and shaking) were optimized for microcultures of *S. cerevisiae* in 96-well plates (see the Supplementary Experimental section). Several specific substrates for different VP catalytic sites were tested to design a suitable screening assay for VP evolution: ABTS, RB5 (Reactive Black 5), VA, Mn^{2+} and DMP (2,6-dimethoxyphenol). In terms of reliability, signal stability and interference with the supernatant from the culture broth, ABTS appeared to be the most appropriate. It is worth noting that this molecule can be very efficiently oxidized by VP at the catalytic tryptophan residue, Trp^{164}, and less efficiently in the haem channel [16]. The ABTS colorimetric assay was adjusted and validated (limit of sensitivity ~5 n-units/ml, coefficient of variance <13 %) to screen for total activity (i.e. the product of functional expression and specific activity for ABTS), and later in the evolution process, this colorimetric assay was adapted to a high-throughput protocol to screen for thermostability [30].

Approximately 9000 clones were explored in six rounds of molecular evolution to improve functional expression and thermostability (Figure 1 and Supplementary Table S1 at http://www.BiochemJ.org/bj/441/bj4410487add.htm). Following a general premise, the whole *α-vpl2* fusion gene was targeted for random mutagenesis and DNA recombination to improve secretion and activity. Once the secretion levels had been considerably improved, mutants were screened at high temperatures in an attempt to transform the VP into a more stable enzyme. Most of the tools employed for library construction were based on *S. cerevisiae* physiology, encouraged by our previous results when using the *in vivo* gap-repair mechanism of this yeast coupled to its high frequency of homologous DNA recombination [31–33]. *In vivo* cloning and/or repair of mutagenic products was tackled by engineering specific overhangs with homologous regions of 30–60 bp that annealed to the linearized vector without altering the ORF (open reading frame). *In vivo* DNA shuffling, IvAM or deletion mutagenesis by IVOE to construct truncated variants were the preferred DNA recombination tools [27,28,34]. Accordingly, error-prone PCR was combined with the aforementioned *in vivo* strategies, which was particularly helpful to overcome the characteristic trade-off between activity and stability when evolving towards thermal stability [35,36]. In order to enhance further the complexity of the library (i.e. the frequency of crossover events between mutant templates), *in vitro* and *in vivo* recombination tools were mixed in the same cycle of evolution (e.g. by combining mutagenic StEP with *in vivo* DNA shuffling). Up to three re-screenings were incorporated in the evolution protocol to rule out the presence of false positives.

Directed evolution for functional expression

The first four cycles of evolution aimed to enhance the secretion of the VP in *S. cerevisiae* (Figure 1 and Supplementary Table S1). The TAI (total activity improvement) over the parental VPL2 obtained from large-scale fermentations was ~129-fold (the TAI value represents the enhancement of both ABTS specific activity and secretion; Supplementary Table S2 at http://www.BiochemJ.org/bj/441/bj4410487add.htm). The breakdown of the TAI value reflected a 51.6-fold improvement in functional expression and a 2.5-fold increase in ABTS oxidation activity with respect to the parental enzyme. The secretion of the most strongly expressed variant (R4 mutant) was 21.6 mg/l, to the best of our knowledge the highest functional expression reported to date for a high-redox potential peroxidase (from ligninolytic fungi).

During evolution, several mutations were introduced in the α-factor prepro-leader (up to eight mutations that included two synonymous ones, four in the pre-leader and four in the pro-leader), although consecutive cycles of DNA recombination ruled out all of them (Figure 1 and Supplementary Table S1). Hence the native signal sequence of the α-factor appeared to drive efficient secretion of the mature R4 mutant in yeast and it did not need further adjustment to successfully export the VP polypeptide. The mutation rate coupled with DNA recombination was highly tuned to generate approximately one mutation per round of evolution on average (i.e. the R4 expression mutant harboured four mutations after four cycles of evolution; Figure 1). Therefore the accumulation of neutral or deleterious mutations was almost completely avoided, which was advantageous in terms of identifying the roles of specific mutations. The four mutations E37K, V160A, T184M and Q202L harboured in the R4 mutant provided an amino acidic backbone responsible for the enhancement in functional expression and ABTS oxidation activity. Three of these four mutations (E37K, V160A and T184M) were introduced independently in different first generation mutants (the 11H10, 15G9 and 4B1 variants

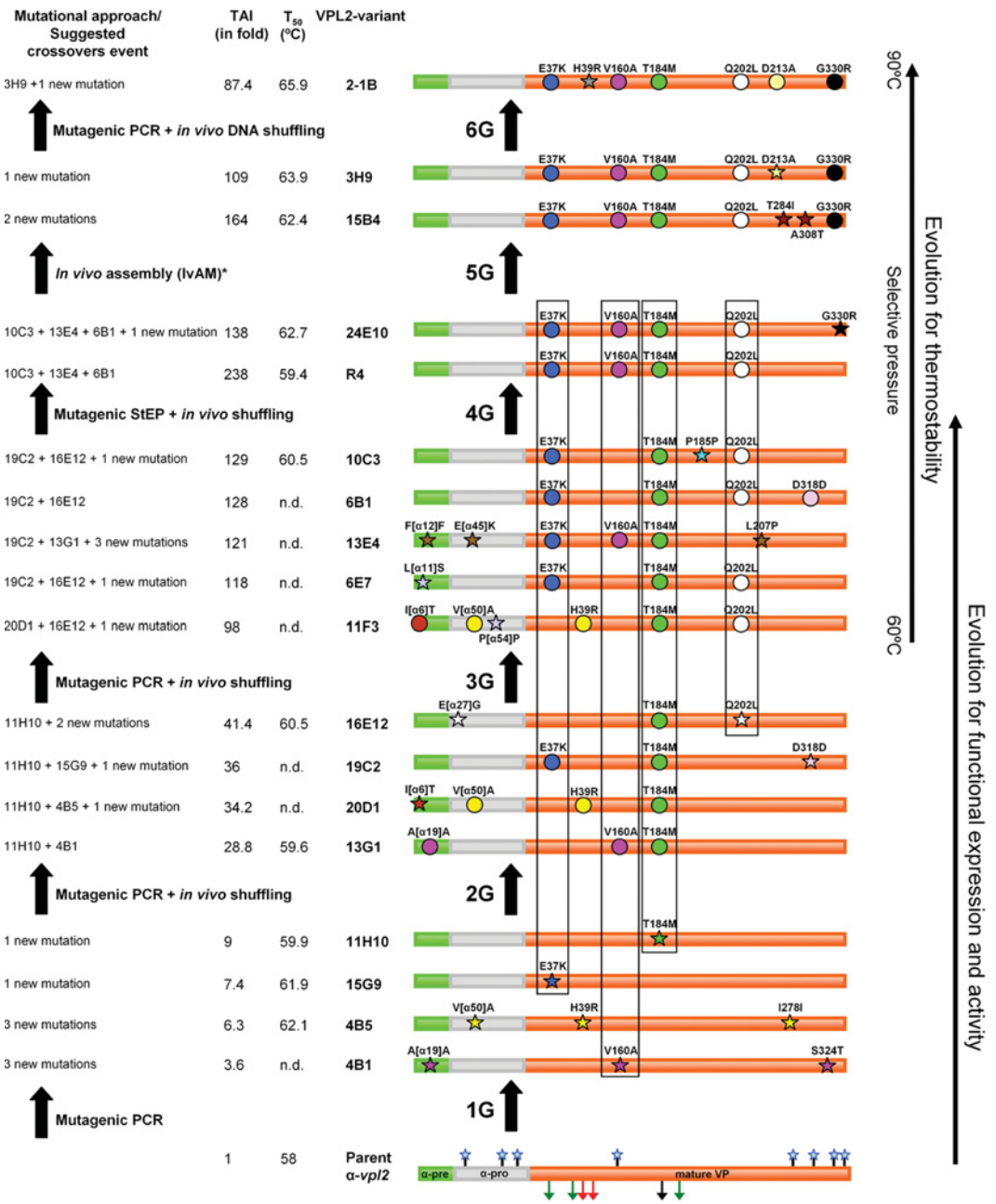

Figure 1 Laboratory evolution of the *α-vpl2* fusion gene

The properties targeted for evolution were secretion (from first to fourth generation) and thermal stability (from fourth to sixth generation). In the fourth generation, secretion and thermal stability were combined during the screening. The α-factor pre-leader is represented in green, the α-factor pro-leader is in grey, and the mature VP is in orange. In the parent *α-vpl2*, the glycosylation sites are represented as blue stars, the Mn^{2+}-binding site (Glu^{36}, Glu^{40} and Asp^{175}) is indicated by green arrows, the catalytic Trp^{164} is marked by a black arrow and the H_2O_2-binding site (from the distal side, Arg^{43} and His^{47}) is shown by red arrows. New mutations are depicted as stars and accumulated mutations are shown as circles. The amino acid backbone for secretion is highlighted in boxes. TAI indicates the improvement in VP activity detected in *S. cerevisiae* microcultures for each mutant when compared with the parental *α-vpl2*. The breakdown of the TAI into specific activity and expression for the best secretion variant is represented in Supplementary Table S2 at http://www.BiochemJ.org/bj/441/bj4410487add.htm. The suggested crossover events and the T_{50} values are included (n.d., not determined). See also Supplementary Table S1 at http://www.BiochemJ.org/bj/441/bj4410487add.htm.

that had TAI values ranging from 9- to 3.6-fold over parental type), whereas Q202L came from the best mutant of the second generation, the 16E12 variant. The DNA recombination approach enabled us to recreate crossover events in such a way that these mutations, discovered early in the evolution pathway, represented a common and well-conserved scaffold on which new thermostable variants could be constructed from the fourth round onwards.

The extra N-terminal sequence

The α-factor prepro-leader fusion proteins are processed in yeast by: (i) a signal peptidase acting on the pre-leader during the translocation of the nascent secretory protein at the endoplasmic reticulum membrane; and (ii) the action of *STE13* and *KEX2* proteases in the Golgi compartment to remove the pro-leader (Supplementary Figure S1A at http://www.BiochemJ.org/bj/441/bj4410487add.htm) [29,37,38].

It has been reported that when high levels of fusion protein secretion are achieved with the α-factor prepro-leader, alternative processing occurs such that extracellular proteins contain a dipeptide spacer sequence linked to the N-terminus. This effect is attributed to the fact that the yeast produced insufficient *STE13* protease to process the high levels of heterologous proteins expressed from these synthetic genes. When we sequenced the N-terminal end of the R4 mutant overexpressed by *S. cerevisiae*, an extra acidic N-terminal sequence (EAEA, Glu-Ala-Glu-Ala) led the original mature protein, confirming that *STE13* failed to adequately process the pro-leader (Supplementary Figure S1B).

We decided to delete the portion of our synthetic gene encoding the spacer dipeptide (Supplementary Figure S1C), engineering a truncated version of the R4 mutant by IVOE deletion mutagenesis [28]. This strategy took advantage of the eukaryotic *S. cerevisiae* machinery by designing specific overhangs between fragments with homologous regions that tolerated the splicing of the truncated products between each other and with the linearized vector, giving rise to an autonomously replicating plasmid (see the Supplementary Experimental section and Supplementary Figure S2 at http://www.BiochemJ.org/bj/441/bj4410487add.htm). The new variant was produced and purified, and the N-terminus was sequenced to verify that it was correctly processed and secreted without the *STE13* cleavage site (i.e. only through *KEX2* protease activity; Supplementary Figure S1C). However, the secretion levels were reduced $\sim$60 % upon deletion of the EAEA sequence (Supplementary Table S3 at http://www.BiochemJ.org/bj/441/bj4410487add.htm). Since the removal of the charged spacer peptide linked the fusion directly to the Lys-Arg processing site, making it a poor substrate for the *KEX2* protease, an acidic environment in the proximity of the *KEX2* cleavage site would appear to be important for secretion. Similar effects have been observed with other fusions, such as the α-factor leader–interferon-α1, in which the intracellular accumulation and secretion of unprocessed and partially processed forms occurred [39]. The truncated R4 variant behaved similarly to its extra N-terminal sequence counterpart in terms of spectroscopic characteristics, kinetic parameters and stability (including pH-activity profiles and temperature or pH stability), indicating that the N-terminal extension had little or no impact on the biochemical properties of the mutant VPs (Table 1, Figure 3, Supplementary Table S3 and Supplementary Figure S3 at http://www.BiochemJ.org/bj/441/bj4410487add.htm). Therefore the R4 mutant containing the N-terminal sequence was subjected to further engineering.

Directed evolution for thermal stability

After considerably augmenting the levels of secretion by evolution, our next goal was to tailor a more thermostable VP. Accordingly, further rounds of evolution were carried out and screened with a high-throughput thermostability assay, based on the ratio of residual activity/initial activity in combination with the estimated T_{50} values [30] (see the Supplementary Experimental section for details). The selection pressure was progressively increased from 60 °C (fourth cycle) to 80 °C and 90 °C in the fifth and sixth generations respectively. This approach was possible because the improvements accomplished in each generation were sufficient to retain >30 % of residual activity making them suitable to evolve stability. The T_{50} (i.e. the temperature at which the enzyme retains 50 % of its activity after 10 min of incubation) shifted $\sim$2 °C per round of evolution for thermostability (Figure 2A), attaining a final T_{50} of 66 °C in the most thermostable mutant, the 2-1B variant (with a global improvement in T_{50} of 8 °C over the parental VPL2). Interestingly,

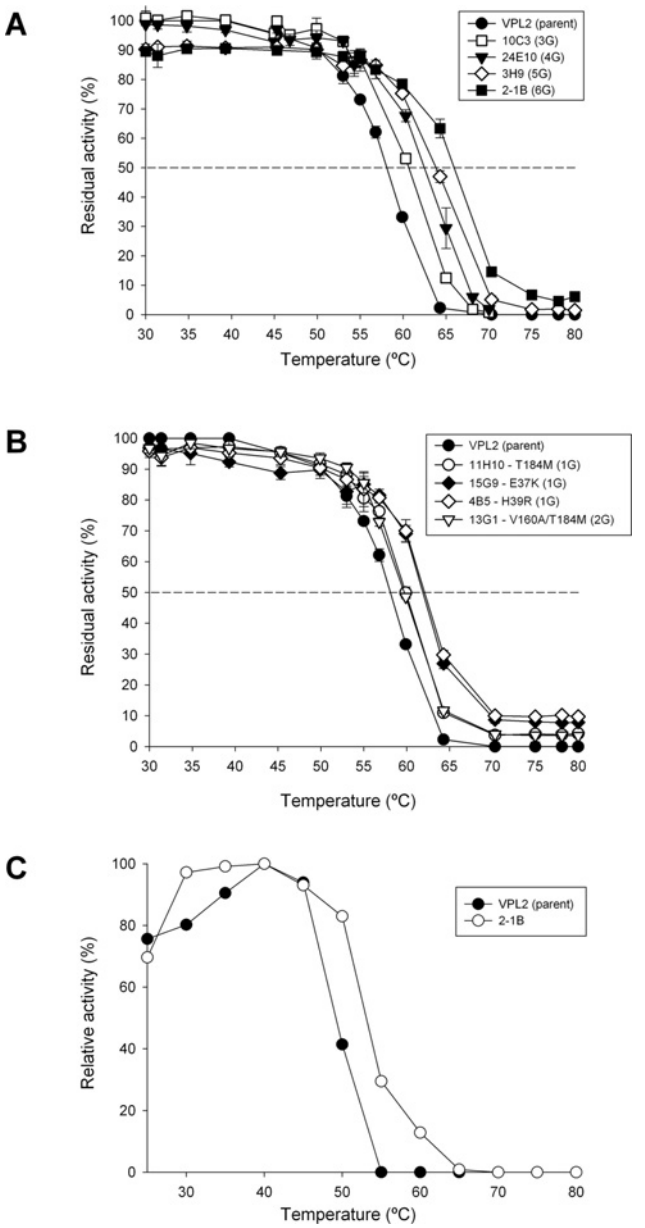

Figure 2 Thermostability of evolved VPs

(**A**) T_{50} profiles of mutants from the third to sixth generations. (**B**) T_{50} profiles of mutants from the first and second generations. (**C**) Thermo-activity (optimum temperature for activity) of parental VPL2 and the 2-1B mutant. Results are means $\pm$ S.D. for three independent experiments.

an improvement of $\sim$2 °C in T_{50} was detected in the third generation 10C3 mutant when compared with the original parental VPL2, despite the fact that the thermal stability was not targeted during the first three rounds of evolution, only secretion (Figures 1 and 2A). Hence some of the mutations discovered during the *in vitro* evolution for expression also displayed improved stability.

Intrigued by this result, we evaluated the T_{50} values in several variants of the first and second generation that harboured beneficial mutations finally inherited by the 10C3 mutant. The improvements in stability could be precisely attributed to each mutation under study as, at this primary stage of evolution, most of the mutations appeared individually in the mutants or in combination with other mutations that were either silent or located at the signal leader, and that did not affect stability (Figure 1 and Supplementary Table S1). Accordingly, the T_{50} of the 11H10

Table 1 Kinetic parameters for parent type and evolved variants of VPL2 expressed in *S. cerevisiae*

Kinetic constants were estimated in 100 mM sodium tartrate buffer containing 0.1 mM H_2O_2 at pH 3.5 for ABTS, DMP and RB5, and at pH 5.0 for Mn^{2+}. H_2O_2 kinetic constants were estimated using ABTS as reducing substrate at the corresponding saturated conditions and taking into account the reaction stoichiometry (one H_2O_2 molecule is reduced for oxidation of two ABTS molecules).

Substrate	Kinetic constants	VPL2 parent type	R4 mutant	2-1B mutant
ABTS (low efficiency)	K_m (mM)	0.54 ± 0.05	0.056 ± 0.003	0.034 ± 0.004
	k_{cat} (s^{-1})	220 ± 30	365 ± 6	850 ± 40
	k_{cat}/K_m ($mM^{-1} \cdot s^{-1}$)	410 ± 30	6480 ± 280	25000 ± 2100
DMP (low efficiency)	K_m (mM)	32 ± 6	6.5 ± 0.5	2.5 ± 0.2
	k_{cat} (s^{-1})	98 ± 7	58 ± 1	97 ± 1
	k_{cat}/K_m ($mM^{-1} \cdot s^{-1}$)	3.1 ± 0.4	9.1 ± 0.5	39 ± 2
RB5	K_m (mM)	0.007 ± 0.0007	0.0066 ± 0.0004	0.0055 ± 0.0006
	k_{cat} (s^{-1})	11.8 ± 0.5	10.6 ± 0.2	9.4 ± 0.4
	k_{cat}/K_m ($mM^{-1} \cdot s^{-1}$)	1670 ± 100	1600 ± 65	1700 ± 140
Mn^{2+}	K_m (mM)	0.045 ± 0.007	0.12 ± 0.01	4.3 ± 0.3
	k_{cat} (s^{-1})	54 ± 1	75 ± 1	98 ± 2
	k_{cat}/K_m ($mM^{-1} \cdot s^{-1}$)	1190 ± 180	630 ± 50	23 ± 1
H_2O_2	K_m (mM)	0.051 ± 0.009	0.20 ± 0.02	0.8 ± 0.1
	k_{cat} (s^{-1})	135 ± 5	490 ± 15	1720 ± 70
	k_{cat}/K_m ($mM^{-1} \cdot s^{-1}$)	2650 ± 370	2400 ± 160	2260 ± 305

Table 2 Biochemical features of parent and evolved variants

n.d., not determined.

Biochemical and spectroscopic feature	VPL2	R4 mutant	2-1B mutant
Molecular mass (Da)*	35257.6	35243.7	35317.9
Molecular mass (Da)†	38618.4	38600.0	38761.4
Degree of glycosylation (%)	9	9	9
Thermal stability, T_{50} (°C)	58	59.4	65.9
pI	4.6	4.6	4.6
Optimum pH	3.0	3.5	4.0
R_Z (A_{410}/A_{280})	2	4	4
Soret region (nm)	407	407	407
Charge transference band, CT1 (nm)	n.d.	504	503
Charge transference band, CT2 (nm)	631	638	638

*Estimated from amino acid composition.
†Estimated by MALDI–TOF-MS.

mutant containing the T184M mutation and the 15G9 mutant containing the E37K mutation improved 2–4 °C over VPL2, which corroborated the stabilizing effect of T184M and E37K mutations (Figures 1 and 2B). The T_{50} remained constant when the 13G1 mutant from the second generation was compared with 11H10, indicating that the V160A mutation did not affect thermal stability. It is also notable that the H39R mutation (found for the first time in the 4B5 mutant from the first generation) was lost during the recombination events that took place in the fourth round, although it was rediscovered in the final cycle for thermal stability (in the 2-1B mutant; Figure 1). The T_{50} of the 4B5 mutant was 4 °C higher than that of the parental type, which confirmed that the H39R mutation also had a strong influence on protein stability during secretion (Figure 2B).

Enhanced thermostability often coincides with improved thermo-activity (T_a) and/or a widening of the T_a range [40]. The 2-1B mutant had the same T_a (defined as the optimal temperature for activity) as the parental VPL2 at 40 °C, although the range of temperature at which the enzyme is highly active was broader after artificial selection (2-1B retaining over 80 % of relative activity in the range from 30 to 50 °C as opposed to the range from 30 to 45 °C for the parental type; Figure 2C). Thus the relative activity at 50 °C of the 2-1B mutant was double that of the parental type at the same temperature. Generally, when thermostability is improved, there is an inherent trade-off between stability and activity, with the concomitant detrimental effect on the specific activity. This is basically due to the fact that stabilizing mutations are not necessarily beneficial for activity, but, rather, they may confer robustness on the protein structure that compromises flexibility in some cases and, consequently, turnover rates. Indeed, the TAI was reduced from 129-fold (10C3 mutant, 3G) to 87-fold (2-1B mutant, 6G) from the fourth to sixth round of evolution (Figure 1). However, as might be expected, this reduction did not drastically affect the kinetics, but, rather, expression above all. With all of the substrates tested (except for Mn^{2+}, where several stabilizing mutations were located around the Mn^{2+}-binding site, see below), the catalytic efficiencies were either improved (at the haem channel site, with ~4-fold improvements for ABTS or DMP) or conserved (at the catalytic Trp^{164}) when compared with the R4 mutant (Table 1).

In general terms, the secretion backbone generated for functional expression helped tolerate the introduction of a new set of stabilizing mutations during evolution towards thermal stability without compromising the kinetics. This was particularly noticeable in the fourth generation when screening for total activity and thermostability was combined in the same cycle (Figure 1). For the first time, all of the fourth generation VPL2 variants selected bought together the E37K, V160A, T184M and Q202L mutations to produce the most active mutant R4. The related 24E10 mutant also selected harboured an additional G330R mutation that, while impeding large gains in total ABTS oxidation activity, increased its thermostability by >2 °C (Figure 1). The DNA recombination method used in this cycle (mutagenic StEP in combination with *in vivo* DNA shuffling) favoured the joining of the four mutations beneficial for total activity, which buffered the effect of incorporating the stabilizing mutation G330R in the same template. Therefore a more thermostable mutant with activity similar to that of the parental types was created.

Characterization of evolved VPs

The parental and evolved R4 and 2-1B VPs were purified and their averaged molecular masses were measured by MALDI–TOF-MS (matrix-assisted laser-desorption ionization–time-of-flight MS) and found to marginally differ from their

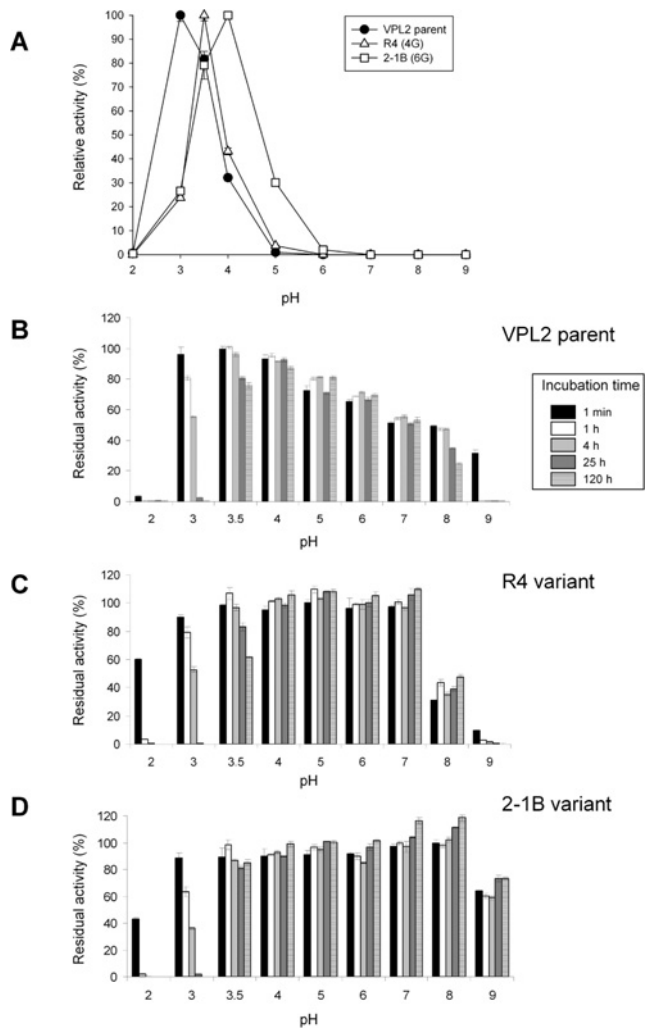

Figure 3 Activity and stability against pH

(**A**) pH-activity profile for the parental VPL2, R4 and 2-1B mutants. Activities were measured in 100 mM B&R (Britton and Robinson) buffer at different pHs with 2 mM ABTS and 0.1 mM H_2O_2. VP activity was normalized to the optimum activity value, and results are means ± S.D. for three independent experiments. pH stability of the parental VPL2 (**B**), the R4 (**C**) and the 2-1B mutants (**D**). Enzyme samples were incubated in 100 mM B&R buffer at different pH values, and the residual activity was measured in 100 mM sodium tartrate buffer (pH 3.5) containing 2 mM ABTS and 0.1 mM H_2O_2. Results are means ± S.D. for three independent experiments. See also Table 2 and Supplementary Figure S4 at http://www.BiochemJ.org/bj/441/bj4410487add.htm.

expected masses (Table 2). The other biochemical features (pI 4.6; ∼9% glycosylation) also remained unchanged in the mutant VPs (Table 2 and Supplementary Figure S4 at http://www.BiochemJ.org/bj/441/bj4410487add.htm). Unlike other proteins expressed heterologously in *S. cerevisiae* that are hyperglycosylated upon secretion, the low sugar content of the parental VPL2 and the mutants probably reflects the short residence in the Golgi compartment that is associated with the ease of exocytosis by yeast. The spectroscopic characteristics of VP variants expressed by *S. cerevisiae* were similar to those of VP from *P. eryngii* or the *in vitro* refolded VP from *E. coli* inclusion bodies (Table 2 and Supplementary Figure S4D). Thus the absorption spectrum showed a maximum in the Soret region and two charge transference bands (CT1 and CT2) that are characteristic of Fe^{3+} in a high-spin state. The pH-activity profile was shifted in the course of evolution and while the parental VPL2 displayed an optimum pH for activity at 3.0, this value rose to 3.5 and 4.0 for the R4 and 2-1B variants respectively (Figure 3A). Together with this unexpected change, the stability at alkaline pH values was notably improved in the thermostable 2-1B variant (Figures 3B–3D). When maintained for 120 h at pH 9.0, the 2-1B variant conserved ∼60% of its residual activity as it was very stable in the pH range 3.5–9. In contrast, the parental VPL2 (from yeast) was very unstable at pH 9.0, losing nearly all of its residual activity after 1 h at this pH. Similar alkaline instability has been reported for the wild-type VP produced by *P. eryngii* as well as for the *Aspergillus*-expressed recombinant enzyme, being related to the loss of structural Ca^{2+} ions (as shown by enzyme stability in Ca^{2+}-containing buffer) [23].

Kinetic constants were assessed using an array of substrates that bind to the different catalytic sites of VP (Table 1). The substrates ABTS and DMP are both oxidized with high efficiency at the catalytic Trp^{164} and less efficiently at the haem channel site. Substrate RB5 is exclusively oxidized at Trp^{164}, whereas the substrate Mn^{2+} is only oxidized at the Mn^{2+} oxidation site [16]. The R4 mutant had an improved affinity for ABTS and DMP at the haem channel with a 10-fold lower K_m and almost 2-fold higher k_{cat} for ABTS that enhanced its k_{cat}/K_m 16-fold compared with VPL2. This improvement prevented the measurement of ABTS oxidation at the catalytic Trp^{164} since the kinetics of ABTS oxidation at the haem channel masked the plots for its oxidation at this site. However, the k_{cat}/K_m values for RB5 at the catalytic Trp^{164} were readily measured and they were similar to those of the parental VPL2 (∼1600 $mM^{-1} \cdot s^{-1}$), indicating that the improvement in activity was mainly concentrated at the haem channel site. Similar behaviour was detected for the thermostable 2-1B mutant with RB5 as substrate, yet the k_{cat}/K_m for ABTS was much improved at the haem channel site (over 61-fold better than the parental type). In contrast, and even though the k_{cat} for Mn^{2+} was slightly improved over the course of evolution, the Mn^{2+}-binding site was negatively affected by the mutations (see the structural analysis of the mutations below), with a 2.6- and 94-fold enhancement of the K_m for Mn^{2+} for R4 and 2-1B respectively. We chose ABTS for the screening as this molecule can be oxidized at both the haem channel site and the catalytic tryptophan residue, thereby avoiding the tendency to lose performance at the different catalytic sites. Indeed, activity at both sites was fairly well conserved or even substantially improved during evolution. The fall in Mn^{2+} activity underscores the fact that all of the properties not addressed in the screen could drift. For future applications in which Mn^{2+} activity might be required, the kinetics of the enzyme with this specific substrate can be enhanced by directed evolution or semi-rational approaches.

Stability of the evolved VPs against peroxide

Peroxidases are inhibited by excess of H_2O_2 and the *Pleurotus* VP is no exception [41]. Although this inhibition is caused by relatively large molar excesses of H_2O_2 (with respect to enzyme concentration), it results in substantial activity losses when the enzyme is in the absence of a reducing substrate. The explanation for such inhibition is found in the peroxidase catalytic cycle, which includes a highly reactive two-electron oxidized species (compound I, a porphyrin radical Fe^{4+}=O complex) that, under turnover conditions, is reduced back to the resting state (via compound II, Fe^{4+}=O haem). In the absence of reducing substrate, compound I reacts with H_2O_2, resulting in compound III (a Fe^{3+}–superoxide complex) formation and then in irreversible inactivation due to the haem/protein oxidative degradation, as reported for ligninolytic and other peroxidases [42,43]. Comparing peroxide stability between different peroxidases is not straightforward because the process is strongly dependent on

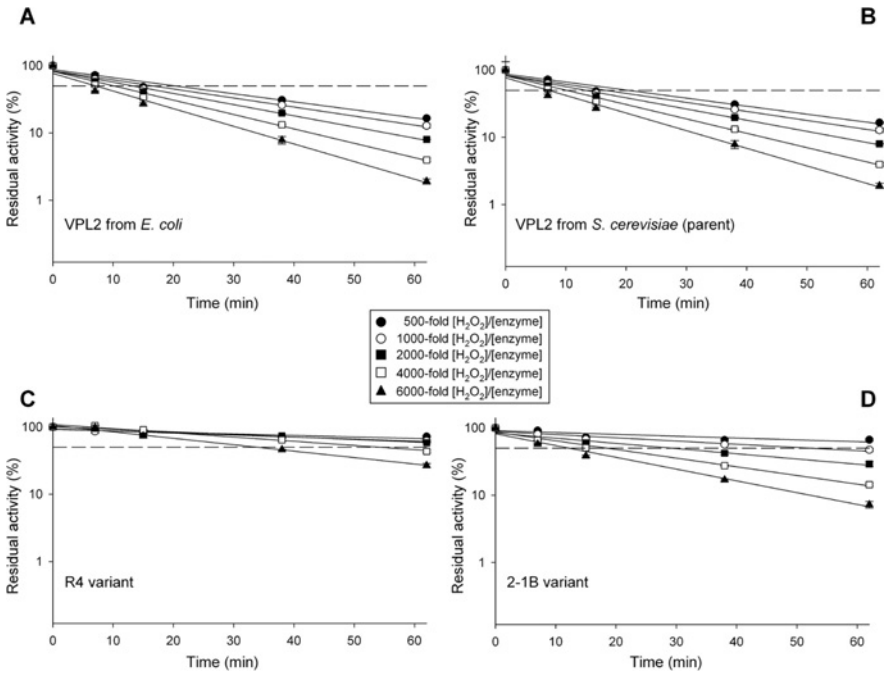

Figure 4 Inactivation of parental and VP mutants at different H_2O_2/enzyme ratios

(**A**) VPL2 from *E. coli* after *in vitro* refolding. (**B**) Functional expression in *S. cerevisiae* of the parental VPL2, (**C**) the R4 and (**D**) 2-1B mutant. The purified VPs (0.06 μM) were incubated at room temperature (24 °C) in 20 mM B&R (Britton and Robinson) buffer containing different H_2O_2 concentrations. The following [H_2O_2]/[VP] molar ratios were assayed: ●, 500-fold; ○, 1000-fold; ■, 2000-fold; □, 4000-fold; ▲, 6000-fold. The residual activity was measured with 2 mM ABTS and 0.1 mM H_2O_2 in 100 mM sodium tartrate buffer (pH 3.5). The residual activity refers to the corresponding VP variant incubated in the absence of H_2O_2, taking into account the final concentration of H_2O_2 for each assay. Results are means ± S.D. for three independent experiments. The broken line indicates 50 % of the residual activity. See also Supplementary Figure S5 at http://www.BiochemJ.org/bj/441/bj4410487add.htm.

pH; nevertheless, wild-type VP susceptibility would be of the same order as other ligninolytic peroxidases (60 % inactivation after 1 h of incubation with 250 H_2O_2 equivalents at pH 4.5, and 90 % inactivation at pH 3.0) [41]. Inactivation by their oxidizing substrate is an important problem to be overcome for biotechnological application of peroxidases, since some loss of activity is produced by H_2O_2 even under steady-state operation conditions, and in this context has been referred to as a suicide inactivation of the enzyme [43–45]. Although this problem has yet to be fully resolved, it has been examined by controlling the addition of H_2O_2 by sensors, by co-immobilization with glucose oxidase to generate H_2O_2 *in situ* coupled to the oxidation of glucose, as well as through site-directed mutagenesis and directed evolution (with low- and high-redox potential peroxidases, but not VPs) [46–53].

In the course of evolution, we detected a dramatic shift in the K_m for H_2O_2. The peroxide k_{cat} was inferred from ABTS oxidation at the haem channel site (taking into account the stoichiometry of the reaction: one molecule of H_2O_2 is reduced by oxidizing two substrate molecules; Table 1 and Supplementary Figure S5 at http://www.BiochemJ.org/bj/441/bj4410487add.htm). Indeed, the R4 and 2-1B mutants reduced their affinity for H_2O_2 4- and 15-fold respectively, without the catalytic efficiency being modified. This means that the evolved VP can operate at higher H_2O_2 concentrations with a significant improvement in turnover rates (k_{cat}, molecules of peroxide reduced per molecule of VP per s) from 135 s^{-1} for VPL2 to 1720 s^{-1} for 2-1B. In contrast, the 2–7-fold increases in K_m for H_2O_2 attained by engineering H_2O_2 stability in bacterial dye-decolorizing peroxidases by site-directed mutagenesis of methionine residues resulted in reductions in k_{cat} and subsequent catalytic efficiency k_{cat}/K_m [53]. Thus R4 and 2-1B worked efficiently in the presence of high concentrations of H_2O_2, showing specific activities with ABTS as high as 3530 and 11 300 units/mg respectively, when estimated using saturating H_2O_2 conditions (i.e. at concentrations of 2.0 and 7.6 mM for R4 and 2-1B respectively, representing 10-fold the H_2O_2 K_m of each variant). Under these conditions, the total ABTS-oxidation activity of the R4 mutant secreted into the culture broth was ~57 000 units/l, to date the highest value reported for any peroxidase as far as we are aware.

The half lives in the presence of H_2O_2 ($t_{1/2}$ H_2O_2) were assessed at several H_2O_2/enzyme molar ratios (Figure 4). Both the R4 and 2-1B mutants significantly improved their peroxide stability relative to VPL2. The $t_{1/2}$ H_2O_2 of R4 and 2-1B at a H_2O_2/enzyme molar ratio of 4000:1 was enhanced from 10 min for VPL2 to 53 and 19 min respectively (Figure 4). In contrast, the K_m for H_2O_2 for 2-1B was 4- and 16-fold higher than for R4 and VPL2 (Table 1). This apparent catalytic inconsistency is probably a consequence of the different experimental conditions used to measure K_m for H_2O_2 (steady-state conditions in the presence of both peroxidase oxidizing and reducing substrates) and $t_{1/2}$ H_2O_2 (no reducing substrate present). The enhanced K_m for H_2O_2 detected in R4 and 2-1B suggests that the kinetic constants of the transient state has been altered by directed evolution of VP, the estimation of which could provide additional information on the mechanisms underlying peroxide stability. These changes may affect different stages of the VP catalytic cycle (i.e. from the resting state to compound I, or its derivative compound II). In fact, any subtle modification in the balance between these intermediates could vary the overall catalytic cycle, affecting the formation of compound III, which is the main precursor for peroxidase inactivation by H_2O_2, as described above. Possibly, the improved oxidative stability is a side effect of laboratory evolution, suggesting a potential use of our mutants to further select for VP variants with improved stability against H_2O_2.

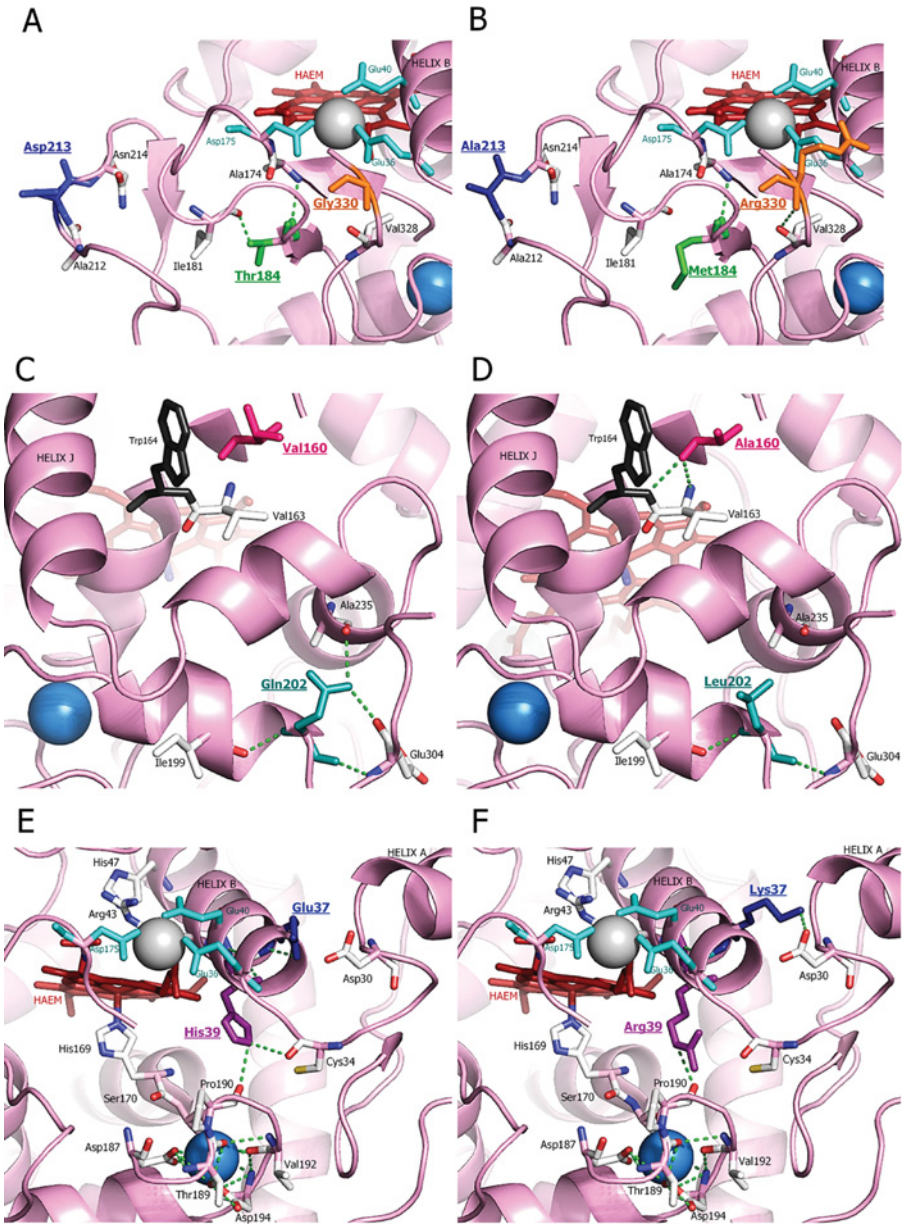

Figure 5 Structural examination of the selected mutations in VPL2

The haem group is represented in red, the catalytic Trp^{164} is in black, and the Mn^{2+}-binding site formed by acidic residues Glu^{36}, Glu^{40} and Asp^{175} is in blue. Grey sphere, Mn^{2+}; blue sphere, Ca^{2+}. (**A** and **B**) Mutations G330R (in orange and underlined), D213A (in blue and underlined) and T184M (in green and underlined). (**C** and **D**) Mutations V160A (in red and underlined) and Q202L (in green and underlined). (**E** and **F**) Mutations H39R (in violet and underlined) and E37K (in blue and underlined). The residues involved in the co-ordination of the proximal Ca^{2+} (Ser^{170}, Asp^{187}, Thr^{189}, Val^{192} and Asp^{194}) are highlighted. Based on PDB code 3FJW (parental VPL2) and modelled with the mutations introduced by directed evolution.

Structural analysis of mutations

The mutations introduced by directed evolution were mapped using the crystal structure of glycosylated VP isolated from *P. eryngii* (PDB code 3FJW; Supplementary Figure S6 at http://www.BiochemJ.org/bj/441/bj4410487add.htm). In this structure, Thr^{184}, Glu^{37} and Val^{160} mutated in R4 are partially exposed to the solvent and distributed in different regions of the protein (Supplementary Figure S6). In contrast, the mutated Leu^{202} occupies an internal position in the VP molecule. Upon inspection of the VP structure, the Thr^{184} mutation may interrupt a hydrogen bond with the neighbouring Ile^{181}, relieving possible structural tension in this region (Figures 5A and 5B). This change might also cause reorientation of the hydrogen-bonded Ala^{174} and adjoining Asp^{175} that constitutes one of the three carboxy residues of the Mn^{2+}-binding site, possibly explaining the increased K_m for Mn^{2+} by R4 (Table 1). The Q202L mutation may interrupt two hydrogen bonds with Ala^{235} and Glu^{304}. This residue is located deep in the protein, at the end of the last β-strand in the enzyme, which is followed by a long C-terminal tail (Supplementary Figure S6). The possible changes in the hydrogen-bonding structure provoked by the Q202L mutation in this area might enhance the structural flexibility of the protein, improving its secretion (Figures 5C and 5D). The E37K mutation increased the T_{50} by 4 °C (Figure 2B). The side-chain carboxy group of Glu^{37} is hydrogen-bonded to the backbone amide proton of Glu^{36} (both residues located in helix B; Figures 5E and 5F). However, inspection of the protein model suggests that the resulting Lys^{37} may establish a

salt bridge with the adjacent Asp^{30} of helix A. This new interaction could pack the two neighbouring A and B helices more tightly, which may improve stability [54]. Moreover, Glu^{36} is one of the three acidic residues forming the Mn^{2+}-binding site, and it seems plausible that helix B could shift slightly due to this mutation, varying the relative position of Glu^{36} with respect to the other two acidic residues. This shift could ultimately affect the geometry of the co-ordination sphere of the Mn^{2+} ion and, consequently, the affinity for this substrate [18] (Table 1). Interestingly, helix B also harbours the residues involved in H_2O_2 binding (His^{47} and Arg^{43}). Any subtle change in the position of this helix relative to the haem cofactor could affect peroxide binding, and, indeed, the K_m for H_2O_2 in the R4 mutant was 15-fold higher than that of the parental VPL2 (Table 1 and Supplementary Figure S5). Finally, the V160A mutation seems to create two new hydrogen bonds (with Trp^{164} and Val^{163}; Figures 5C and 5D), without affecting either the kinetics at the catalytic Trp^{164} (Table 1) or stability (Figure 2B). The change in this position could be related with more correct polypeptide maturation in *S. cerevisiae*.

The remaining mutations discovered during the evolution to improve thermal stability were also located at the surface of the protein (G330R, D213A and H39R). Gly^{330} is situated at the C-terminal tail of VP, the most mobile region in the protein (Supplementary Figure S6). According to our model, the G330R mutation seems to produce a new hydrogen bond with Val^{328} (Figures 5A and 5B), which could stabilize this area (the T_{50} was enhanced by 2.2 °C upon mutation; Figure 1). Asp^{213} is very exposed to solvent in the most external part of the haem channel (Figures 5A and 5B). The change of a negative residue for a neutral one at this position would help VP to accommodate negatively charged substrates, like ABTS, to be oxidized at the haem edge. It is likely that a change in the polarity of this region might suppress unfolding at higher temperatures. The H39R mutation was discovered at different points of the evolution route and indeed, the secretion mutant 4B5 and the final 2-1B thermostable variant incorporated this mutation in the first and last cycle of evolution respectively. As discussed above, this mutation considerably enhances the stability of the enzyme, improving secretion and thermal stability (Figures 1 and 2B). In native VP, His^{39} is hydrogen-bond to Pro^{190}, acting as a bridge between helix B and the loop containing the proximal Ca^{2+} ion (one of the two structural Ca^{2+} conserved in all Class-II peroxidases [10]). In fact, this proline residue is contiguous with Thr^{189}, one of the five residues involved in the co-ordination of the proximal Ca^{2+} ion in VP (together with Ser^{170}, Asp^{187}, Val^{192} and Asp^{194}). Differences in the strength of the hydrogen bonds between His^{39} and Pro^{190} in native VP and between Arg^{39} and Pro^{190} in 2-1B (Figures 5E and 5F) could be related to the improvement in thermal (and alkaline) resistance of the latter variant by modifying the stability of the proximal Ca^{2+}-binding site. This effect is supported by the fact that the first-generation 4B5 variant (containing only the H39R beneficial mutation) also showed improved stability (Figures 1 and 2B).The suggested changes in the proximal Ca^{2+} loop after mutation are in good agreement with the reported role for the protein stability of the two structural Ca^{2+} ions, as for LiP and VP among other Class-II peroxidases [13,55,56]. The H39R mutation may also break down the hydrogen bond with Cys^{34} (Figures 5E and 5F), which in turn could affect the distance between helix B and the haem domain, modifying the binding of peroxide (Supplementary Figure S5). It is also worth noting that this mutation may affect the oxidation of Mn^{2+} in the 2-1B variant (exhibiting a K_m value 100-fold higher than that of the parental VPL2), enhancing the effect previously described for the E37K mutation since both Arg^{39} and Lys^{37} are contiguous with Glu^{40}, which, along with Glu^{36} and Asp^{175}, contributes to the Mn^{2+}-binding site (Table 1). A summary of the different characteristics (such as location, distance to the catalytic sites and interactions affected) of the seven residues that were mutated during VP directed evolution is provided in Supplementary Table S4 at http://www.BiochemJ.org/bj/441/bj4410487add.htm.

Conclusions

VPs are a typical example of generalist enzymes with phylogenetic sequence comparisons indicating that they are related to MnP and LiP. In principle, VP has adapted through natural selection to combine many catalytic phenotypes from its related peroxidases. Indeed, modern VPs probably possess a broader substrate specificity than their ancestral progenitors [14]. Given their intrinsic enzymatic promiscuity, it is likely that VPs have the capacity to evolve novel catalytic properties, making them a potentially powerful model enzyme to engineer by molecular evolution towards specialized functions. *S. cerevisiae* is considered by many to be the preferred eukaryotic model organism for molecular and cell biology, with this versatility making it a highly useful expression host in directed protein evolution studies [28,46,57]. Indeed, in the present study, we have demonstrated the usefulness of *S. cerevisiae* for evolving VP variants via laboratory evolution strategies to select for more stable and active forms, possibly serving as a suitable platform to tailor VPs with targeted catalytic attributes [58]. Recently, new laccases have been engineered by artificial evolution, strengthening the array of ligninolytic enzymes available for different potential applications [31,59]. These evolutionary models could be employed as a biomolecular toolbox in order to address both traditional problems and new challenges in synthetic biology that have so far hindered the practical use of VPs and other high-redox-potential oxidoreductases: from inactivation by H_2O_2 to the construction of artificial operons of evolved laccases and VPs for the directed evolution of whole ligninolytic cell factories in yeast.

AUTHOR CONTRIBUTION

Eva Garcia-Ruiz carried out all of the laboratory evolution experiments. David Gonzalez-Perez helped in the biochemical characterization of evolved variants. Francisco Ruiz-Dueñas and Angel Martínez contributed to the structure–function analysis of the mutations and helped with the writing and the revision of the paper. Miguel Alcalde conceived the project, supervised its development and wrote the paper.

ACKNOWLEDGEMENTS

We thank Rita Getzlaff from the Helmholtz Centre for Infection Research (HZI, Braunschweig, Germany) for sequence analyses. We thank Dr Francisco J. Plou from the ICP (CSIC, Madrid, Spain) for assistance with the HPLC purification.

FUNDING

This study is based upon work funded by European Union Projects [grant numbers NMP2-CT-2006-026456-Biorenew, FP7-KBBE-2010-4-26537-Peroxicats and COST Action CM0701] and National projects [grant numbers BIO2010-19697 and BIO2008-01533]. We also thank NeuronBiopharma for financial support through Research Contracts [grant numbers 020401070029, Profit Program and 020401070004, Idea Program]. E.G.-R. was supported by a Biorenew grant, D.G.-P. was supported by a Peroxicats contract, and F.J.R.-D. was supported by the Ministerio de Cienca e Innovación (MICINN) Ramón y Cajal Program.

REFERENCES

1 Martínez, A. T., Ruiz-Dueñas, F. J., Martínez, M. J., del Río, J. C. and Gutiérrez, A. (2009) Enzymatic delignification of plant cell-wall: from nature to mill. Curr. Opin. Biotechnol. **20**, 348–357

2 Ruiz-Dueñas, F. J. and Martínez, A. T. (2009) Microbial degradation of lignin: how a bulky recalcitrant polymer is efficiently recycled in nature and how we can take advantage of this. Microbial Biotechnol. **2**, 164–177
3 Kamm, B. and Kamm, M. (2007) Biorefineries: multi product processes. Adv. Biochem. Eng./Biotechnol. **105**, 175–204
4 Orts, W. J., Imam, S., Glenn, G. M., Inglesby, M., Wong, D., Guttman, M. and Samac, D. A. (2004) Envisioning biorefineries based on utilization of lignocellulosic straws and bagasses. 227th National Meeting of the American Chemical Society, Anaheim, CA, U.S.A., 28 March–1 April 2004, Abstract Cell 192
5 Alcalde, M., Ferrer, M., Plou, F. J. and Ballesteros, A. (2006) Environmental biocatalysis: from remediation with enzymes to novel green processes. Trends Biotechnol. **24**, 281–287
6 Xu, F. (2005) Applications of oxidoreductases: recent progress. Industr. Biotechnol. **1**, 38–50
7 Camarero, S., Sarkar, S., Ruiz-Dueñas, F. J., Martínez, M. J. and Martínez, A. T. (1999) Description of a versatile peroxidase involved in natural degradation of lignin that has both Mn-peroxidase and lignin-peroxidase substrate binding sites. J. Biol. Chem. **274**, 10324–10330
8 Martínez, M. J., Ruiz-Dueñas, F. J., Guillén, F. and Martínez, A. T. (1996) Purification and catalytic properties of two manganese-peroxidase isoenzymes from *Pleurotus eryngii*. Eur. J. Biochem. **237**, 424–432
9 Ruiz-Dueñas, F. J., Martínez, M. J. and Martínez, A. T. (1999) Molecular characterization of a novel peroxidase isolated from the ligninolytic fungus *Pleurotus eryngii*. Mol. Microbiol. **31**, 223–236
10 Martínez, A. T. (2002) Molecular biology and structure–function of lignin-degrading heme peroxidases. Enzyme Microb. Technol. **30**, 425–444
11 Rainio, A., Maijala, P., Hildén, K. and Hatakka, A. (2008) A novel peroxidase from the white-rot fungus *Cerrena unicolor*. Peroxidase 2008, Tampere, Finland 20–23 August 2008, Abstract PX-S10-5
12 Moreria, P. R., Duez, C., Dehareng, D., Antunes, A., Almeida-Vara, E., Frère, J.-M., Malcata, F. X. and Duarte, J. C. (2005) Molecular characterisation of a versatile peroxidase from a *Bjerkandera* strain. J. Biotechnol. **118**, 339–352
13 Verdín, J., Pogni, R., Baeza, A., Baratto, M. C., Basosi, R. and Vázquez-Duhalt, R. (2006) Mechanism of versatile peroxidase inactivation by Ca^{2+} depletion. Biophys. Chem. **121**, 163–170
14 Hofrichter, M., Ullrich, R., Pecyna, M. J., Liers, C. and Lundell, T. (2010) New and classic families of secreted fungal heme peroxidases. Appl. Microbiol. Biotechnol. **87**, 871–897
15 Martínez, A. T. (2007) High redox potential peroxidases. In Industrial Enzymes: Structure, Function and Applications (Polaina, J. and MacCabe, A. P., eds), pp. 475–486, Springer, Berlin
16 Ruiz-Dueñas, F. J., Morales, M., García, E., Miki, Y., Martínez, M. J. and Martínez, A. T. (2009) Substrate oxidation sites in versatile peroxidase and other basidiomycete peroxidases. J. Exp. Bot. **60**, 441–452
17 Ruiz-Dueñas, F. J., Morales, M., Mate, M. J., Romero, A., Martínez, M. J., Smith, A. T. and Martínez, A. T. (2008) Site-directed mutagenesis of the catalytic tryptophan environment in *Pleurotus eryngii* versatile peroxidase. Biochemistry **47**, 1685–1695
18 Ruiz-Dueñas, F. J., Morales, M., Pérez-Boada, M., Choinowski, T., Martínez, M. J., Piontek, K. and Martínez, A. T. (2007) Manganese oxidation site in *Pleurotus eryngii* versatile peroxidase: a site-directed mutagenesis, kinetic and crystallographic study. Biochemistry **46**, 66–77
19 Ruiz-Dueñas, F. J., Pogni, R., Morales, M., Giansanti, S., Mate, M. J., Romero, A., Martínez, M. J., Basosi, R. and Martínez, A. T. (2009) Protein radicals in fungal versatile peroxidase: catalytic tryptophan radical in both Compound I and Compound II and studies on W164Y, W164H and W164S variants. J. Biol. Chem. **284**, 7986–7994
20 Cañas, A. and Camarero, S. (2010) Laccases and their natural mediators: biotechnological tools for sustainable eco-friendly processes. Biotechnol. Adv. **28**, 694–705
21 Ruiz-Dueñas, F. J., Martínez, M. J. and Martínez, A. T. (1999) Heterologous expression of *Pleurotus eryngii* peroxidase confirms its ability to oxidize Mn^{2+} and different aromatic substrates. Appl. Environ. Microbiol. **65**, 4705–4707
22 Eibes, G. M., Lu-Chau, T. A., Ruiz-Dueñas, F. J., Feijoo, G., Martínez, M. J., Martínez, A. T. and Lema, J. M. (2009) Effect of culture temperature on the heterologous expression of *Pleurotus eryngii* versatile peroxidase in *Aspergillus* hosts. Bioprocess Biosyst. Eng. **32**, 129–134
23 Lú-Chau, T. A., Ruiz-Dueñas, F. J., Camarero, S., Feijoo, G., Martínez, M. J., Lema, J. M. and Martínez, A. T. (2004) Effect of pH on the stability of *Pleurotus eryngii* versatile peroxidase during heterologous production in *Emericella nidulans*. Bioprocess Biosyst. Eng. **26**, 287–293
24 Mohorcic, M., Bencina, M., Friedrich, J. and Jerala, R. (2009) Expression of soluble versatile peroxidase of *Bjerkandera adusta* in *Escherichia coli*. Bioresour. Technol. **100**, 851–858
25 Pérez-Boada, M., Doyle, W. A., Ruiz-Dueñas, F. J., Martínez, M. J., Martínez, A. T. and Smith, A. T. (2002) Expression of *Pleurotus eryngii* versatile peroxidase in *Escherichia coli* and optimisation of *in vitro* folding. Enzyme Microb. Technol. **30**, 518–524
26 Zhao, H. M., Giver, L., Shao, Z. X., Affholter, J. A. and Arnold, F. H. (1998) Molecular evolution by staggered extension process (StEP) *in vitro* recombination. Nat. Biotechnol. **16**, 258–261
27 Zumárraga, M., Camarero, S., Shleev, S., Martínez-Arias, A., Ballesteros, A., Plou, F. J. and Alcalde, M. (2008) Altering the laccase functionality by *in vivo* assembly of mutant libraries with different mutational spectra. Proteins **71**, 250–260
28 Alcalde, M. (2010) Mutagenesis protocols in *Saccharomyces cerevisiae* by *in vivo* overlap extension. Methods Mol. Biol. **634**, 3–14
29 Brake, A. J. (1990) α-Factor leader-directed secretion of heterologous proteins from yeast. Methods Enzymol. **185**, 408–421
30 García-Ruiz, E., Maté, D., Ballesteros, A., Martínez, A. T. and Alcalde, M. (2010) Evolving thermostability in mutant libraries of ligninolytic oxidoreductases expressed in yeast. Microb. Cell Fact. **9**, 17
31 Mate, D., Garcia-Burgos, C., Garcia-Ruiz, E., Ballesteros, A. O., Camarero, S. and Alcalde, M. (2010) Laboratory evolution of high-redox potential laccases. Chem. Biol. **17**, 1030–1041
32 Zumárraga, M., Bulter, T., Shleev, S., Polaina, J., Martínez-Arias, A., Plou, F. J., Ballesteros, A. and Alcalde, M. (2007) *In vitro* evolution of a fungal laccase in high concentrations of organic cosolvents. Chem. Biol. **14**, 1052–1064
33 Bulter, T., Alcalde, M., Sieber, V., Meinhold, P., Schlachtbauer, C. and Arnold, F. H. (2003) Functional expression of a fungal laccase in *Saccharomyces cerevisiae* by directed evolution. Appl. Environ. Microbiol. **69**, 987–995
34 Alcalde, M., Zumárraga, M., Polaina, J., Ballesteros, A. and Plou, F. J. (2006) Combinatorial saturation mutagenesis by *in vivo* overlap extension for the engineering of fungal laccases. Comb. Chem. High Throughput Screening **9**, 719–727
35 Bloom, J. D. and Arnold, F. H. (2009) In the light of directed evolution: pathways of adaptive protein evolution. Proc. Natl. Acad. Sci. U.S.A. **106**, 9995–10000
36 Romero, P. A. and Arnold, F. H. (2009) Exploring protein fitness landscapes by directed evolution. Nat. Rev. Mol. Cell Biol. **10**, 866–876
37 Brake, A. J., Merryweather, J. P., Coit, D. G., Heberlein, U. A., Masiarz, F. R., Mullenbach, G. T., Urdea, M. S., Valenzuela, P. and Barr, P. J. (1984) α-Factor-directed synthesis and secretion of mature foreign proteins in *Saccharomyces cerevisiae*. Proc. Natl. Acad. Sci. U.S.A. **81**, 4642–4646
38 Romanos, M. A., Scorer, C. A. and Clare, J. J. (1992) Foreign gene expression in yeast: a review. Yeast **8**, 423–488
39 Zsebo, K. M., Lu, H. S., Fieschko, J. C., Goldstein, L., Davis, J., Duker, K., Suggs, S. V., Lai, P. H. and Bitter, G. A. (1986) Protein secretion from *Saccharomyces cerevisiae* directed by the prepro-α-factor leader region. J. Biol. Chem. **261**, 5858–5865
40 Cirino, P. C. and Georgescu, R. (2003) Screening for thermostability. Methods Mol. Biol. **230**, 117–125
41 Böckle, B., Martínez, M. J., Guillén, F. and Martínez, A. T. (1999) Mechanism of peroxidase inactivation in liquid cultures of the ligninolytic fungus *Pleurotus pulmonarius*. Appl. Environ. Microbiol. **65**, 923–928
42 Wariishi, H. and Gold, M. H. (1989) Lignin peroxidase compound III: formation, inactivation, and conversion to the native enzyme. FEBS Lett. **243**, 165–168
43 Valderrama, B., Ayala, M. and Vázquez-Duhalt, R. (2002) Suicide inactivation of peroxidases and the challenge of engineering more robust enzymes. Chem. Biol. **9**, 555–565
44 Timofeevski, S. L., Reading, N. S. and Aust, S. D. (1998) Mechanisms for protection against inactivation of manganese peroxidase by hydrogen peroxide. Arch. Biochem. Biophys. **356**, 287–295
45 Hernández-Ruiz, J., Arnao, M. B., Hiner, A. N. P., García-Canovas, F. and Acosta, M. (2001) Catalase-like activity of horseradish peroxidase: relationship to enzyme inactivation by H_2O_2. Biochem. J. **354**, 107–114
46 Cherry, J. R., Lamsa, M. H., Schneider, P., Vind, J., Svendsen, A., Jones, A. and Pedersen, A. H. (1999) Directed evolution of a fungal peroxidase. Nat. Biotechnol. **17**, 379–384
47 Morawski, B., Quan, S. and Arnold, F. H. (2001) Functional expression and stabilization of horseradish peroxidase by directed evolution in *Saccharomyces cerevisiae*. Biotechnol. Bioeng. **76**, 99–107
48 Miyazaki-Imamura, C., Oohira, K., Kitagawa, R., Nakano, H., Yamane, T. and Takahashi, H. (2003) Improvement of H_2O_2 stability of manganese peroxidase by combinatorial mutagenesis and high-throughput screening using *in vitro* expression with protein disulfide isomerase. Protein Eng. **16**, 423–428
49 Ryu, K., Hwang, S. Y., Kim, K. H., Kang, J. H. and Lee, E. K. (2008) Functionality improvement of fungal lignin peroxidase by DNA shuffling for 2,4-dichlorophenol degradability and H_2O_2 stability. J. Biotechnol. **133**, 110–115
50 Ryu, K., Kang, J. H., Wang, L. S. and Lee, E. K. (2008) Expression in yeast of secreted lignin peroxidase with improved 2,4-dichlorophenol degradability by DNA shuffling. J. Biotechnol. **135**, 241–246

51 Miyazaki, C. and Takahashi, H. (2001) Engineering of the H_2O_2-binding pocket region of a recombinant manganese peroxidase to be resistant to H_2O_2. FEBS Lett. **509**, 111–114
52 Ryan, B. J. and O'Fagain, C. (2007) Effects of single mutations on the stability of horseradish peroxidase to hydrogen peroxide. Biochimie **89**, 1029–1032
53 Ogola, H. J.O., Hashimoto, N., Miyabe, S., Ashida, H., Ishikawa, T., Shibata, H. and Sawa, Y. (2010) Enhancement of hydrogen peroxide stability of a novel *Anabaena* sp. DyP-type peroxidase by site-directed mutagenesis of methionine residues. Appl. Microbiol. Biotechnol. **87**, 1727–1736
54 Musafia, B., Buchner, V. and Arad, D. (1995) Complex salt bridges in proteins: statistical analysis of structure and function. J. Mol. Biol. **254**, 761–770
55 Nie, G. J. and Aust, S. D. (1997) Effect of calcium on the reversible thermal inactivation of lignin peroxidase. Arch. Biochem. Biophys. **337**, 225–231
56 George, S. J., Kvaratskhelia, M., Dilworth, M. J. and Thorneley, R. N. F. (1999) Reversible alkaline inactivation of lignin peroxidase involves the release of both the distal and proximal site calcium ions and bishistidine co-ordination of the haem. Biochem. J. **344**, 237–244
57 Okkels, J. S. (2004) *In vivo* gene shuffling in yeast: a fast and easy method for directed evolution of enzymes. In Enzyme Functionality: Design, Engineering, and Screening (Svendsen, A., ed.), pp. 378–389, Marcel Dekker, New York
58 García, E., Martínez, F. J., Ruiz-Dueñas, F. J., Martínez, A. T. and Alcalde, M. (2010) High redox potential peroxidases designed by directed evolution. Int. Pat. WO/2010/130862
59 Camarero, S., Cañas, A., Martínez, M. J., Martínez, A. T., Ballesteros, A., Plou, F. J., Record, E., Asther, M. and Alcalde, M. (2010) Laccases having high redox potential obtained through directed evolution. Int. Pat. WO/2010/058057

Received 5 July 2011/7 October 2011; accepted 7 October 2011
Published as BJ Immediate Publication 7 October 2011, doi:10.1042/BJ20111199

Biochem. J. (2012) **441**, 487–498 (Printed in Great Britain) doi:10.1042/BJ20111199

SUPPLEMENTARY ONLINE DATA

Directed evolution of a temperature-, peroxide- and alkaline pH-tolerant versatile peroxidase

Eva GARCIA-RUIZ*, David GONZALEZ-PEREZ*, Francisco J. RUIZ-DUEÑAS†, Angel T. MARTÍNEZ† and Miguel ALCALDE*[1]

*Department of Biocatalysis, Institute of Catalysis, CSIC, Cantoblanco, 28049 Madrid, Spain, and †Center for Biological Investigations, CSIC, Ramiro de Maeztu 9, 28040 Madrid, Spain

EXPERIMENTAL

Reagents and enzymes

ABTS, DMP, VA, RB5, haemoglobin from bovine blood, Taq DNA polymerase for random mutagenesis, StEP and the *S. cerevisiae* transformation kit were purchased from Sigma–Aldrich. The *E. coli* XL2-Blue competent cells and the Genemorph II random mutagenesis kit were obtained from Stratagene. The protease-deficient *S. cerevisiae* strain BJ5465 was from LGC Promochem, the uracil-independent and ampicillin-resistance shuttle vector pJRoC30 was a gift from Professor E. H. Arnold at the California Institute of Technology (Caltech), whereas the pGAPZαA vector containing α-factor prepro-leader and the Taq DNA polymerase used to construct the α-*vpl2* fusion were from Invitrogen. The Zymoprep yeast plasmid miniprep kit, Zymoclean gel DNA-recovery kit and the DNA clean and concentrator TM-5 kit were all from Zymo Research. The NucleoSpin® plasmid kit was purchased from Macherey-Nagel and the restriction enzymes BamHI, XhoI, EcoRI and NotI were from New England Biolabs. VPL2 from *E. coli* was prepared by *in vitro* refolding from inclusion bodies as reported previously [25]. All chemicals were reagent-grade purity.

Culture media

Minimal medium contained 100 ml of 6.7 % sterile yeast nitrogen base, 100 ml of 19.2 g/l sterile yeast synthetic drop-out medium supplement without uracil, 100 ml of sterile 20 % raffinose, 1 ml of 25 g/l chloramphenicol and 700 ml of sterile double-distilled water. YP medium contained 10 g of yeast extract, 20 g of peptone and double-distilled water to 650 ml. Flask expression medium contained 720 ml of YP medium, 67 ml of 1 M potassium phosphate buffer (pH 6.0), 111 ml of 20 % galactose, 25 g/l ethanol, 500 mg/l bovine haemoglobin, 1 mM $CaCl_2$, 1 ml of 25 g/l chloramphenicol and double-distilled water to 1 litre. Microplate expression medium contained 720 ml of YP medium, 67 ml of 1 M potassium phosphate buffer (pH 6.0), 111 ml of 20 % galactose, 100 mg/l bovine haemoglobin, 1 ml of 25 g/l chloramphenicol and double-distilled water to 1 litre. YPD solution contained 10 g of yeast extract, 20 g of peptone, 100 ml of 20 % sterile glucose, 1 ml of 25 g/l chloramphenicol and double-distilled water to 1 litre. SC (synthetic complete) drop-out plates contained 100 ml of 6.7 % sterile yeast nitrogen base, 100 ml of 19.2 g/l sterile yeast synthetic drop-out medium supplement without uracil, 20 g of Bacto agar, 100 ml of 20 % sterile glucose, 1 ml of 25 g/l chloramphenicol and double-distilled water to 1 litre.

Construction of pJRoC30-α-*vpl2*

The pGAPZ-αA vector was used as a template to fuse the native *vpl2* with the α-factor prepro-leader. First, the cDNA from *vpl2* (996 bp) excluding the native signal leader was amplified using the following primers: NtEcoRI-direct (5′-CGGAATTCGCAACTTGCGACGACGGACGC-3′) and CtNotl-reverse (5′-AAGGAAAAAAGCGGCCGCTTACGATC-CAGGGACGGGAGG-3′). The target sequences for EcoRI and Notl are underlined. PCRs were performed in a final volume of 50 μl containing 400 nM NecoRI-direct, 400 nM CtNotl-reverse, 0.25 mM dNTPs, 0.05 unit/μl Taq DNA polymerase (Invitrogen), 4 mM $MgCl_2$ and 0.5 ng/μl *vpl2* cDNA. The thermal cycling programme was: 94 °C for 5 min, 55 °C for 5 min, 72 °C for 5 min (1 cycle); 95 °C for 0.35 min, 50 °C for 2 min, 72 °C for 4 min (25 cycles); and 72 °C for 10 min (1 cycle). The amplified *vpl2* was purified by low-melting-point gel extraction and recovered with Zymoclean gel DNA-recovery kit. The *vpl2* product and the pGAPZαA vector were both digested with EcoRI and Notl, and ligated, giving rise to pGAPZ-α-*vpl2*. This construct was used to transform *E. coli* XL2-Blue cells and the product was prepared in large amounts. The pGAPZα-*vpl2* was used to amplify the α-*vpl2* fusion gene with the following primers: NtpJRBamHI-direct (5′-CGCGGATCCATGAGATTTCCTTC-AATTTTTACTGC-3′), which included the BamHI target (underlined); and CtNotL-reverse sequences. PCRs were performed in a final volume of 50 μl containing 400 nM NtpJRBamHI-direct, 400 nM CtNotl-reverse, 0.25 mM dNTPs, 0.05 unit/μl Taq DNA polymerase (Invitrogen), 4 mM $MgCl_2$ and 0.4 ng/μl pGAPZ-α-*vpl2*. The amplified α-*vpl2* fusion was purified and cleaned as described above and then cloned into the pJRoC30 episomal shuttle vector. Both α-*vpl2* and pJRoC30 were linearized with BamHI and NotI, and ligated to generate pJRoC30-α-*vpl2*.

Truncated variant

The extra N-terminal sequence was removed by deletion mutagenesis (R4DEL variant) using IVOE (as summarized in Figure S2 [28]). For the R4DEL mutant, the primers for PCR 1 were RMLN and IVΔSTE13 R (5′-GCAGCATTTGCG-GTGGTGCGTCCGTCGTCGCAAGTTGCTCTTTTCTCGAG-AGATACCCCTTC-3′ which binds to positions 441–465 of pJRoC30-αPM1). The primers for PCR 2 were IVΔEcoRI F (5′-GCAACTTGCGACGACGGACGC-3′ which binds to positions 483–503 of pJRoC30-α-*vpl2*) and RMLC. The products from PCR 1 and PCR 2 have overhangs with homologous regions of 38 bp between each other, and of 40 and 66 bp with the linearized

[1] To whom correspondence should be addressed (email malcalde@icp.csic.es).

vector for *in vivo* cloning. The linearized plasmid (100 ng) was mixed with products from PCR 1 and PCR 2 (400 ng each) and transformed into competent *S. cerevisiae* cells. Individual clones were picked and cultured in 96-well plates (Greiner Bio-One) containing 50 μl of minimal medium per well and subjected to the screening procedure described below. Positive clones were re-screened (see below), the *in vivo* repaired plasmid was recovered, and the truncated fusion gene was confirmed by DNA sequencing.

High-throughput screening assays

Owing to the low levels of secretion, longer induction times in expression medium were used in the first round of evolution (up to 72 h). From the second cycle onwards, expression was sufficiently strong that the time required for protein induction was reduced to 24 h. Moreover, in the first two cycles, the screening was carried out in end-point mode after incubating the supernatants for several hours in the presence of ABTS. As a consequence of the high levels of secretion achieved, from the third generation on the supernatants were diluted 1:10 before screening.

High-throughput screening assays for secretion (total activity)

Individual clones were picked and cultured in 96-well plates (Greiner Bio-One) containing 50 μl of minimal medium per well. In each plate, column number 6 was inoculated with the parental type and one well (H1-control) was inoculated with non-transformed yeast cells as a negative control. The plates were sealed to prevent evaporation and incubated at 30 °C, 225 rev./min and 80 % relative humidity in a humid shaker (Minitron-INFORS, Biogen). After 48 h, 160 μl of expression medium was added to each well and the plates were incubated for 24 h. The plates (master plates) were centrifuged at 3000 ***g*** for 5 min at 4 °C (Eppendorf 5810R centrifuge), and 20 μl of supernatant was transferred from the master plate on to a replica plate using a robot (Liquid Handler Quadra 96-320, Tomtec). The replica plate was filled with 180 μl of 100 mM sodium tartrate buffer (pH 3.5) containing 2 mM ABTS and 0.1 mM H_2O_2. The plates were stirred briefly and the absorption at 418 nm ($\varepsilon_{ABTS}^{\bullet+} = 36\,000$ $M^{-1} \cdot cm^{-1}$) was recorded in the plate reader (SpectraMax Plus 384, Molecular Devices). The plates were incubated at room temperature until the colour developed and the absorption was measured again. Relative activities were calculated from the difference between the absorption after incubation and that of the initial measurement normalized against the parental type and used as a reference in the corresponding plate (the reference parental types were as follows: 1G, α-VPL2; 2G, 11H10; 3G, 16E12; 4G, 10C3; 5G, 24E10; 6G, 3H9).

High-throughput screening assay for thermostability

From the fourth generation onwards, a thermostability assay was incorporated, as described previously [30] with minor modifications. Accordingly, 20 μl of supernatant was transferred to the replica plate from the master plate using the robot. Subsequently, 180 μl of stability buffer (10 mM sodium tartrate buffer, pH 5.0) was added to each replica and they were stirred briefly. The replica plate was duplicated with the help of the robot by transferring 50 μl of the mixtures to a thermocycler plate (Multiply PCR plate without skirt, neutral, Sarstedt) and 20 μl to the initial activity plate. Thermocycler plates were sealed with thermoresistant film (Deltalab) and incubated at the corresponding temperature in a thermocycler (MyCycler, Bio-Rad Laboratories). The incubation took place over 10 min so that the activity assessed was reduced to two-thirds of the initial activity. Afterwards, the thermocycler plates were placed on ice for 10 min and incubated further for 5 min at room temperature. Subsequently, 20 μl of the supernatants were transferred from both the thermocycler and the initial activity plates to new plates to estimate the initial and residual activities in ABTS buffer. The plates were stirred briefly and the ABTS oxidation activity was measured as described in the previous section. The plates were incubated at room temperature until a green colour developed and the absorbance was measured again. The same experiment was performed for both the initial activity plate and the residual activity plate. The relative activity was calculated from the difference between the absorbance after incubation and that of the initial measurement normalized against the parental type in the corresponding plate. Thermostability values were taken as the ratio between the residual and initial activity.

Re-screening

To rule out false positives, two consecutive re-screenings were carried out according to an earlier protocol with some modifications [30]. A third rescreening was incorporated to calculate the T_{50} of the mutants selected from the thermostability assay.

First re-screening. Aliquots (5 μl) of the best clones were removed from the master plates to inoculate minimal medium (50 μl) in new 96-well plates. Columns 1 and 12 (rows A and H) were not used to prevent the appearance of false positives. After 24 h of incubation at 30 °C and 225 rev./min, an aliquot (5 μl) was transferred to the adjacent wells and incubated further for 24 h. Finally, expression medium (160 μl) was added and the plates were incubated for 24 h. Thus each mutant was grown in four wells. The parental types were subjected to the same procedure (lane D, wells 7–11) and the plates were assessed using the same protocol as that used for the screenings described above.

Second re-screening. An aliquot from the wells with the best clones from the first re-screening was inoculated in YPD medium (3 ml), incubated at 30 °C and 225 rev./min for 24 h, and the plasmids from these cultures were recovered (Zymoprep yeast plasmid miniprep kit). As the product of the Zymoprep was very impure and the DNA concentration extracted was very low, the shuttle vectors were transformed into super-competent *E. coli* XL2-Blue cells and plated on to LB (Luria–Bertani)-amp (ampicillin) plates. Single colonies were picked and used to inoculate LB-amp medium (5 ml) and they were grown overnight at 37 °C and 225 rev./min. The plasmids were then extracted (NucleoSpin® plasmid kit) and *S. cerevisiae* was transformed with plasmids from the best mutants and the parental type. Five colonies for each mutant were picked and re-screened as described above.

Third re-screening for thermostability (T_{50}). Fresh transformants of selected mutants and of the parental types were cultured (10 ml) in a 100 ml flask for VP production. The supernatants were assayed for thermostability to accurately estimate their T_{50} using 96/384-well gradient thermocyclers. Appropriate dilutions of supernatants were prepared with the help of the robot such that aliquots (20 μl) produced a linear response in kinetic mode, and for each point in the gradient scale, aliquots (50 μl) from both selected mutants and the parental types were used. A temperature gradient profile ranging from 30 to 80 °C was established and, after 10 min of incubation, samples were chilled on ice for 10 min and incubated further at room temperature for 5 min. Finally, aliquots (20 μl) were removed and subjected to the same ABTS-based colorimetric

assay described above for the screening. Thermostability values were deduced from the ratio between the residual activities incubated at different temperatures and the initial activity at room temperature.

Production and purification of VP variants

Production of VPs in *S. cerevisiae*

A single colony from the *S. cerevisiae* clone containing the parental or mutant *vp* gene was picked from a SC drop-out plate, inoculated in minimal medium (10 ml) and incubated for 48 h at 30 °C and 225 rev./min (Micromagmix shaker). An aliquot of cells was removed and used to inoculate minimal medium (50 ml) in a 500 ml flask (at a D_{600} of 0.25). The cells completed two growth phases (6–8 h) and then expression medium (450 ml) was inoculated with the pre-culture (50 ml) in a 2 litre baffled flask (D_{600} of 0.1). After incubating for 48 h at 30 °C and 225 rev./min (maximal VP activity; $D_{600} = 28$–30), the cells were recovered by centrifugation at 4600 ***g*** for 15 min at 4 °C on an Avanti J-E centrifuge, Beckman Coulter) and the supernatant was double-filtered (through both a glass filter and then a nitrocellulose membrane of 0.45 μm pore size).

Purification

VPs were purified by FPLC (fast protein liquid chromatography) (LCC-500CI instrument, GE Healthcare) and HPLC [Waters 600E System with a Varian PDA (photodiode array) detector]. The crude extract was first submitted to a fractional precipitation with ammonium sulfate (50 %, first cut) and after removing the pellet, the supernatant was again precipitated with ammonium sulfate (65 %, second cut). The final pellet was recovered in 20 mM piperazine buffer (buffer P, pH 5.5), and the sample was filtered and loaded on to the FPLC coupled with a strong anion-exchange column (HiTraP QFF, GE Healthcare) pre-equilibrated with buffer P. The proteins were eluted with a linear gradient from 0 to 1 M of NaCl in two phases at a flow rate of 1 ml/min: from 0 to 25 % over 50 min and from 25 to 100 % over 10 min. Fractions with VP activity were pooled, concentrated, dialysed against buffer P and purified further by HPLC–PDA coupled with a 10 μm high-resolution anion-exchange Biosuite Q (Waters) pre-equilibrated with buffer P. The proteins were eluted on a linear gradient from 0 to 1 M NaCl at a flow rate of 1 ml/min in two phases: from 0 to 6 % in 65 min and from 6 to 100 % in 10 min.

For R4DEL, the non-retained fraction (with VP activity) was dialysed against 20 mM Bis-Tris buffer (buffer BT, pH 6.5) and purified by HPLC–PDA coupled with a 10 μm high-resolution anion-exchange Biosuite Q pre-equilibrated with buffer BT. The proteins were eluted with a linear gradient from 0 to 1 M NaCl at a flow rate of 1 ml/min in three phases: from 0 to 7 % in 25 min, from 7 to 9 % in 65 min and from 9 to 100 % in 10 min. The fractions with VP activity were pooled, dialysed against buffer BT and purified by HPLC–PDA under the same conditions described above until Reinheitszahl values (Rz) ~4 were attained. The fractions with VP activity were pooled, dialysed against 10 mM sodium tartrate buffer (pH 5.0), concentrated and stored at −20 °C. Throughout the purification protocol, the fractions were analysed by SDS/PAGE on 12 % gels and the proteins were stained with colloidal Coomassie Blue (Protoblue Safe, National Diagnostics). The concentrations of all crude protein extracts were determined using the Bio-Rad protein reagent and BSA as a standard. Purified VP concentrations were determined by measuring the absorbance at 407 nm ($\varepsilon_{VP} = 150\,000\ M^{-1}\cdot cm^{-1}$).

MALDI–TOF-MS analysis

The MALDI–TOF-MS experiments were performed on an Autoflex III MALDI-TOF-TOF instrument with a smartbeam laser (Bruker Daltonics). The spectra were acquired using a laser power just above the ionization threshold, and the samples were analysed in the positive-ion detection and delayed extraction linear mode. Typically, 1000 laser shots were summed into a single mass spectrum. External calibration was performed, using the BSA from Bruker, covering the range 15 000–70 000 Da. The 2,5-DHAP (2,5-dihydroxyacetophenone) matrix solution was prepared by dissolving 7.6 mg (50 μmol) of 2,5-DHAP in 375 μl of ethanol followed by the addition of 125 μl of 80 mM diammonium hydrogen citrate aqueous solution. To prepare the samples, 2.0 μl of purified enzyme was diluted with 2.0 μl of 2 % trifluoroacetic acid aqueous solution and 2.0 μl of the matrix solution. An aliquot (1.0 μl) of this mixture was spotted on to the stainless steel target and allowed to dry at room temperature.

pI determination

Purified VPs (8 μg each) were subjected to two-dimensional electrophoresis at the Proteomic and Genomic Services from CIB (CSIC, Spain).

N-terminal analysis

Purified VPs were subjected to SDS/PAGE, and the protein bands were blotted on to PVDF membranes. The PVDF membranes were stained with Coomassie Brilliant Blue R-250, after which the enzyme bands were excised and processed for N-terminal amino acid sequencing on a precise sequencer at the Core facilities of the Helmholtz Centre for Infection Research.

Determination of thermostability (T_{50})

The thermostability of the different VP samples was estimated by assessing their T_{50} values using 96/384-well gradient thermocyclers. Appropriate VP dilutions were prepared with the robot such that the aliquots (20 μl) gave rise to a linear response in the kinetic mode. The samples (50 μl) were then used for each point in the gradient scale and a temperature gradient profile ranging from 30 to 80 °C was established as follows: 30.0, 31.4, 34.8, 39.3, 45.3, 49.9, 53, 55, 56.8, 59.9, 64.3, 70.3, 75, 78.1 and 80 °C. After 10 min of incubation, samples were chilled on ice for 10 min and incubated further at room temperature for 5 min. Afterwards, aliquots (20 μl) were subjected to the ABTS-based colorimetric assay described above for screening. The thermostability values were deduced from the ratio between the residual activities incubated at different temperatures and the initial activity at room temperature.

Kinetic parameters

As reported previously [17], steady-state enzyme kinetics were determined using the following molar absorption coefficients: ABTS product, $\varepsilon_{418} = 36\,000\ M^{-1}\cdot cm^{-1}$; DMP product, $\varepsilon_{469} = 27\,500\ M^{-1}\cdot cm^{-1}$ (in reference to the substrate concentration); RB5, $\varepsilon_{598} = 50\,000\ M^{-1}\cdot cm^{-1}$; Mn^{3+}-tartrate, $\varepsilon_{238} = 6500\ M^{-1}\cdot cm^{-1}$.

DNA sequencing

Plasmids containing VP variants were sequenced with an ABI 3730 DNA Analyzer/Applied Biosystems Automatic

Sequencer from Secugen. The primers were designed with Fast-PCR software (University of Helsinki) as follows: RMLN; 3R-direct (5′-GTTCCATCATCGCGTTCG-3′); 5F-reverse (5′-GGATTCCTTTCTTCTTGG-3′) and RMLC.

Protein modelling

The structural model of wild-type VPL2 (purified from *P. eryngii* culture) at a resolution of 2.8 Å (1 Å = 0.1 nm) (PDB code 3FJW) was used to map the mutations, and the 1.33 Å crystal structure of non-glycosylated VP from *E. coli* (PDB code 2BOQ) was used for comparison (only 0.36 Å root mean square distance between 319 Cα). Mutations selected upon VP evolution were analysed by DeepView/Swiss-Pdb Viewer (GlaxoSmithKline) and the PyMOL Viewer (DeLano Scientific; http://www.pymol.org), and evolved VP variants were modelled using the Swiss-Model protein automated modelling server (http://swissmodel.expasy.org/).

RESULTS

Table S1 Mutations introduced in the directed evolution of *α-vpl2*

Silent mutations are indicated in bold; ○, accumulated mutation; ●, new mutation. Subscript indicates codon usage in *S. cerevisiae*. n.d., not determined.

Mutation		Round of evolution . . .	1G				2G				3G					4G		5G		6G
Amino acid	Codon		11H10	15G9	4B5	4B1	16E12	19C2	20D1	13G1	10C3	6B1	13E4	6E7	11F3	R4	24E10	3H9	15B4	2-1B
I(α6)T	ATT/ACT								●						○					
L(α11)S	TTA/TCA													●						
F(α12)F	TTC_{18}/TTT_{26}												●							
A(α19)A	GCT_{21}/GCC_{12}					●				○										
E(α27)G	GAA/GGA						●													
E(α45)K	GAA/AAA												●							
V(α50)A	GTT/GCT				●				○						○					
P(α54)P	CCA_{18}/CCT_{13}														●					
E37K	GAG/AAG			●				○			○	○	○	○		○	○	○	○	○
H39R	CAC/CGC				●				○						○					●
V160A	GTC/GCC					●				○			○			○	○	○	○	○
T184M	ACG/ATG		●				○	○	○	○	○	○	○	○	○	○	○	○	○	○
P185P	CCA_{18}/CCG_{5}										●									
Q202L	CAA/CTA						●				○	○		○	○	○	○	○	○	○
L207P	CTC/CCC												●							
D213A	GAC/GCC																	●		○
I278I	ATT_{30}/ATC_{17}				●															
T284I	ACC/ATC																		●	
A308T	GCC/ACC																		●	
D318D	GAC_{20}/GAT_{38}							●				○								
S324T	TCC/ACC					●														
G330R	GGA/AGA																●	○	○	○
TAI (fold increase) mutant/parent			9	7.4	6.3	3.6	41.5	36	34.2	28.8	129	128	121	118	98	238	138	109	164	87.4
Thermostability (T_{50}, °C)			59.9	61.9	62.1	n.d.	60.5	n.d.	n.d.	59.6	60.5	n.d.	n.d.	n.d.	n.d.	59.4	62.7	63.9	62.4	65.9

Table S2 Dissection of specific activity and secretion

Total activities and TAI values are calculated from large-scale fermentation experiments. Activities were assessed in 100 mM sodium tartrate buffer (pH 3.5) containing 2 mM ABTS and 0.1 mM H_2O_2.

					Improvement dissection	
Enzyme	Total activity (units/l)	TAI (fold increase)	Units/mg	Secretion levels (mg/l)	Specific activity (fold)	Expression (fold)
VPL2 parent	120	1	283	0.42	1	1
R4 mutant (fourth generation)	15500	129	717	21.6	2.5	51.6

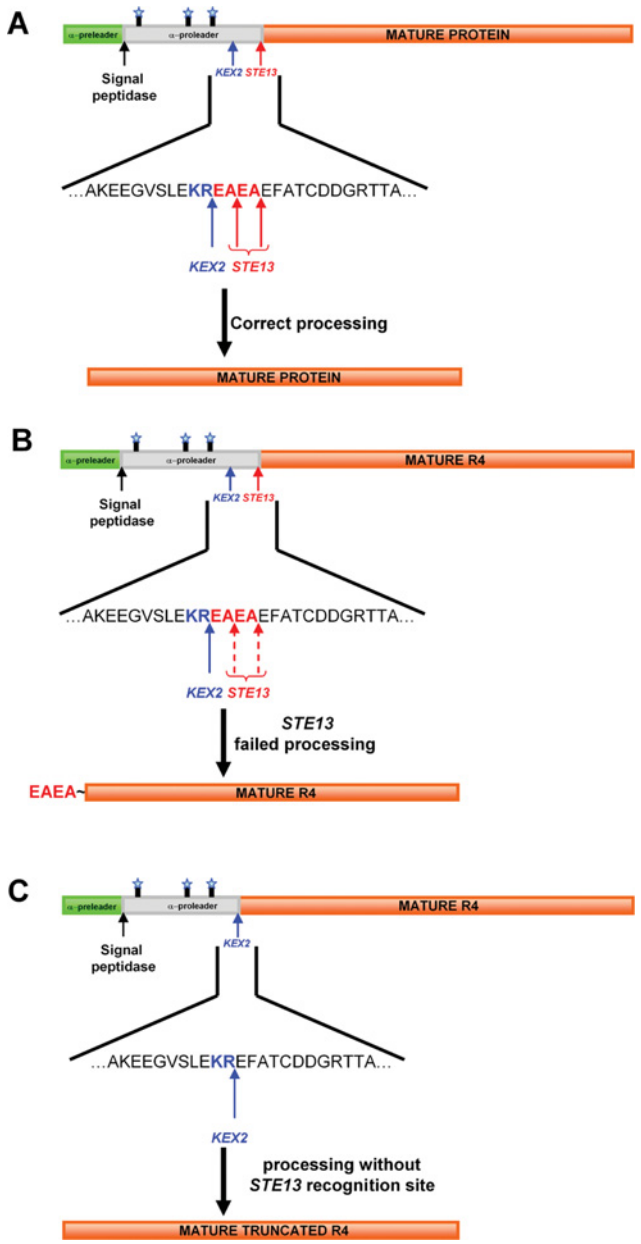

Figure S1 Overexpression of the R4 mutant and the engineering of a truncated variant

(**A**) Correct processing of the α-factor prepro-leader by the signal peptidase, the *KEX2* and *STE13* proteases, during the heterologous expression of a foreign protein in yeast. (**B**) Failed processing of *STE13* and the secretion of mature R4 with an extra N-terminal sequence (in red). (**C**) Fusion construct without the EAEA cleavage site and the action of *KEX2* in mature R4 secretion. The α-factor pre-leader is in green, the α-factor pro-leader is in grey and the mature VP is in orange. Blue stars indicate the glycosylation sites in the pro-leader.

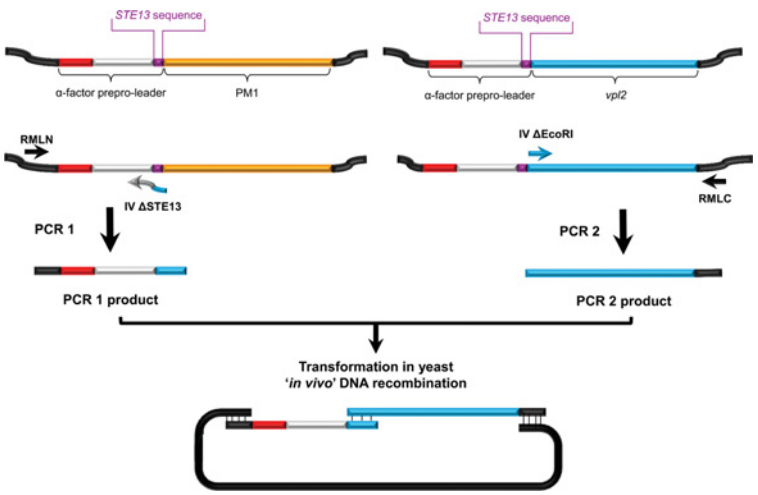

Figure S2 Deletion mutagenesis by IVOE to engineer truncated variants

To amplify the whole α-factor prepro-leader without the *STE13* motif, a construction containing the *PM1* gene instead of the original α-*vpl2* was used as the template to avoid loops and mismatching during PCR with the overhang of the reverse primer IVΔSTE13. The α-factor pre-leader is in red, the α-factor pro-leader is in grey, the *STE13* cleavage site is in purple, the *vpl2* gene is in blue, the *PM1* gene is in orange, and the shuttle vector is in black.

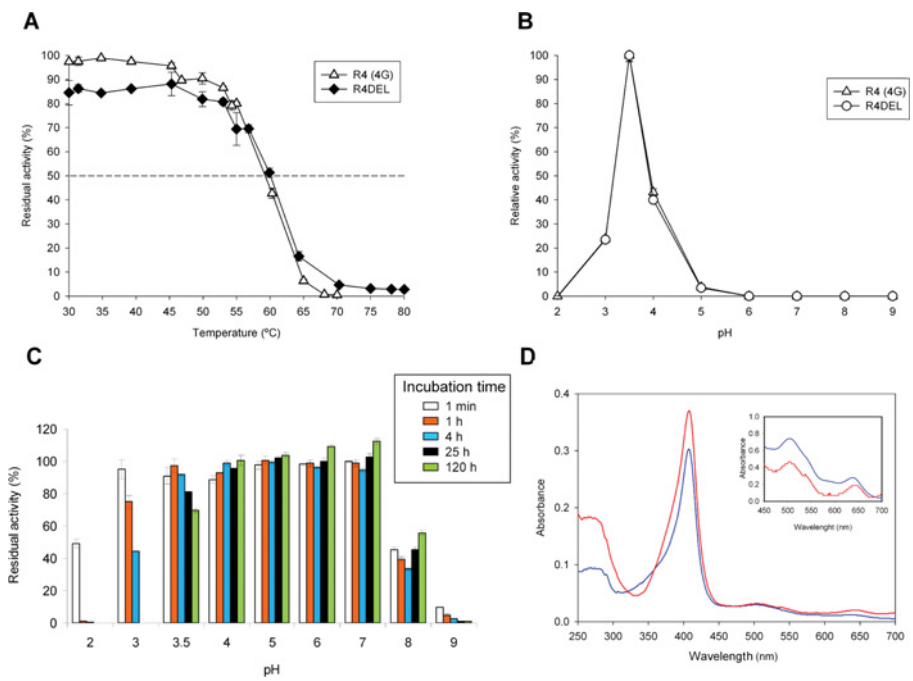

Figure S3 Biochemical characteristics of the R4 truncated variant

(**A**) Thermostability (T_{50}) of the R4 and R4DEL (truncated) mutant. Results are means $\pm$ S.D. for three independent experiments. (**B**) The pH-activity profile for R4 and R4DEL. Activities were measured in 100 mM B&R (Britton and Robinson) buffer at different pH values with 2 mM ABTS and 0.1 mM H_2O_2. VP activity was normalized to the optimum activity value, and results are means $\pm$ S.D. for three independent experiments. (**C**) pH stabilities of R4DEL. Enzyme samples were incubated in 100 mM B&R buffer at different pH values, and the residual activity was measured in 100 mM sodium tartrate buffer (pH 3.5) containing 2 mM ABTS and 0.1 mM H_2O_2. Results are means $\pm$ S.D. for three independent experiments. (**D**) Spectroscopic characteristics of R4 (blue line) and R4DEL (red line). See also Table 1 and Figure 3 of the main text and Table S3.

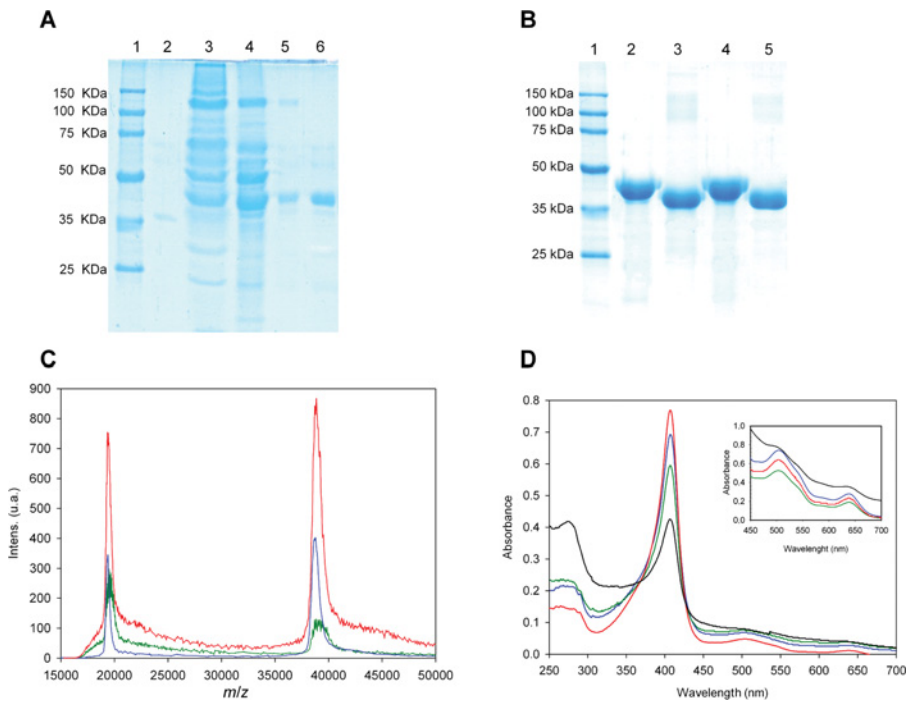

Figure S4 Biochemical characterization of the parental VP and evolved variants

(**A**) SDS/PAGE of the purified R4 mutant. Lanes: 1, protein ladder; 2, VPL2 from *E. coli* after *in vitro* refolding; 3, culture filtrate; 4, $(NH_4)_2SO_4$ precipitate; 5, anion exchange (HiTraP Q FF); 6, high-resolution anion exchange (Biosuite Q). (**B**) N-deglycosylation of R4 and 2-1B variants. Lanes: 1, protein ladder; 2, R4; 3, deglycosylated R4; 4, 2-1B; 5, deglycosylated 2-1B. The purified enzymes were deglycosylated using PNGase F (peptide N-glycosidase F). Samples were resolved by SDS/PAGE (12 % gels) and stained with colloidal Coomassie Blue stain. (**C**) MALDI–TOF mass spectra of VP purified variants (VPL2, green line; R4, blue line; 2-1B, red line). (**D**) Spectroscopic characteristics of VP variants. VPL2 from *S. cerevisiae*, black line; VPL2 from *E. coli* after *in vitro* refolding, red line; R4 variant, blue line; 2-1B variant, green line. See also Table S3.

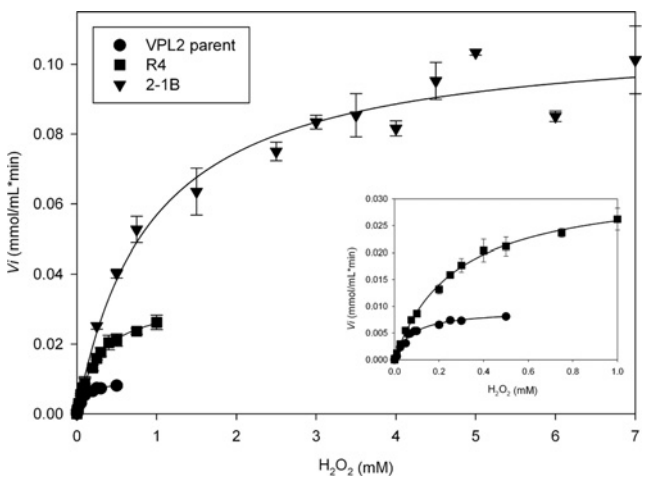

Figure S5 Kinetics for H_2O_2

Estimation of steady-state kinetic constants for H_2O_2 of VPL2, R4 mutant and 2-1B mutant using ABTS as a reducing substrate. The inset shows the low-concentration detail for VPL2 and R4 kinetics, and results are means $\pm$ S.D. of three measurements. Measurements were carried out in 100 mM sodium tartrate buffer (pH 3.5) using 5×10^{-4} μM enzyme and ABTS at concentrations of 5.5 mM (for parental VPL2 and VPL2 from *E. coli* after *in vitro* refolding), 0.6 mM (for the R4 mutant) and 0.5 mM (for the 2-1B mutant).

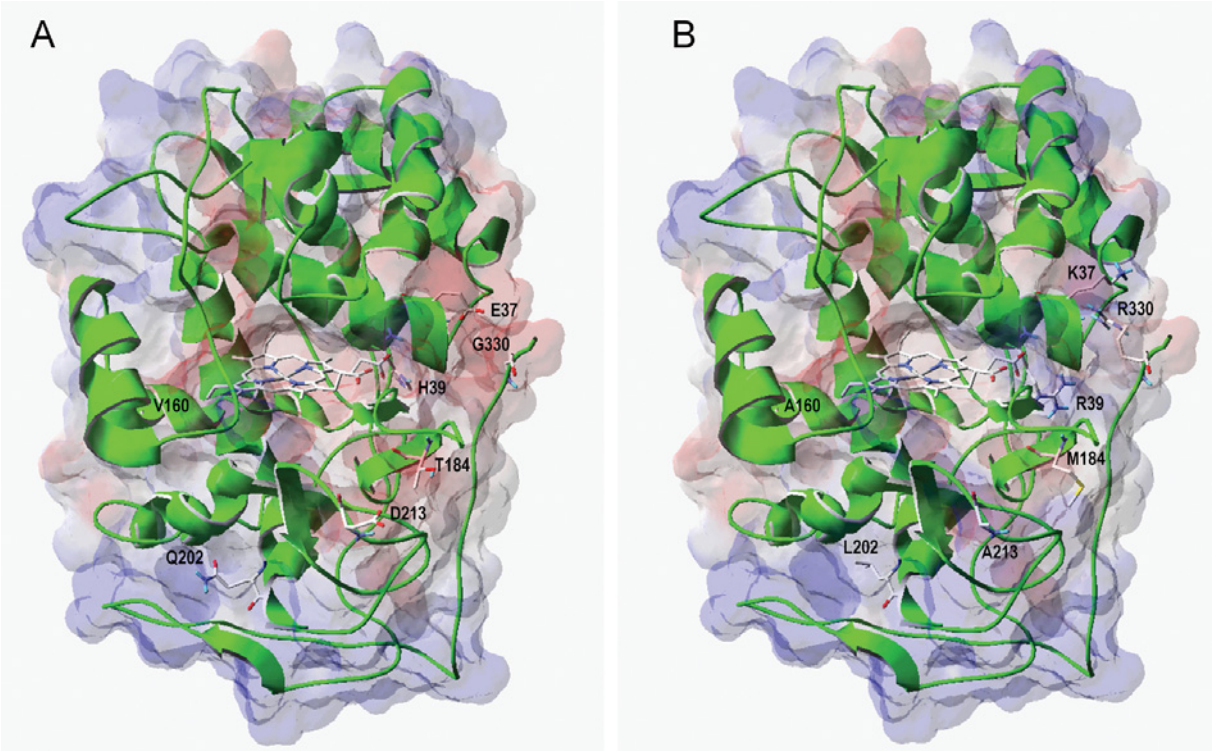

Figure S6 Wild-type VP and 2-1B variant molecular structure

(**A)** Wild-type VPL2 isolated from *P. eryngii* (PDB code 3FJW) indicating the seven residues that were seen to be modified during directed evolution. (**B**) Model for the 2-1B evolved variant including the seven mutations selected. The secondary protein structure (dominated by helices), the position of the haem cofactor [CPK (Corey–Pauling–Koltun) sticks] and the solvent-access surfaces of both proteins (in partially transparent electrostatic-potential colours) are shown.

Table S3 Characteristics of the R4 truncated mutant

Biochemical, spectroscopic and kinetic feature	Value
Molecular mass (Da)*	34567
Molecular mass (Da)†	38100
Degree of glycosylation (%)	9
Thermal stability, T_{50} (°C)	60
Optimum pH	3.5
pI	4.9
R_Z (A_{410}/A_{280})	4
Soret region (nm)	407
Charge transference band, CT1 (nm)	504
Charge transference band, CT2 (nm)	643
Total activity (units/l)‡	4670
Secretion levels (mg/l)	8.84
Kinetics for ABTS (low efficiency)	
K_m (mM)	0.052 ± 0.005
k_{cat} (s^{-1})	520 ± 20
k_{cat}/K_m ($mM^{-1} \cdot s^{-1}$)	9880 ± 620
Kinetics for RB5	
K_m (mM)	0.0043 ± 0.0004
k_{cat} (s^{-1})	10.5 ± 0.3
k_{cat}/K_m ($mM^{-1} \cdot s^{-1}$)	2440 ± 170

*Estimated from amino acid composition.
†Estimated by MALDI–TOF-MS.
‡Activities were assessed in 100 mM sodium tartrate buffer (pH 3.5) containing 2 mM ABTS and 0.1 mM H_2O_2.

Table S4 Mutations in evolved VPs

Mutation	Domain	Secondary structure	Location	Distance to Fe^{3+} (Å)	Distance to Mn^{2+} oxidation site (Å)	Distance to Trp^{164} (Å)	Interactions with surrounding residues*	
							Before mutation	After mutation
E37K	Distal	Helix B	Near Mn^{2+} site	14.29	7.61	21.86	$\underline{Glu^{36}}$, 2×(Ser^{41})	**Asp^{30}**, 2×(Ser^{41})
H39R	Distal	Helix B	Near Mn^{2+} site	9.71	6.74	16.69	$\underline{Cys^{34}}$, Gly^{35}, Glu^{36}, Leu^{42}, Arg^{43}, $\underline{Pro^{190}}$	Gly^{35}, Glu^{36}, Leu^{42}, Arg^{43}, **Pro^{190}**
V160A	Distal	Helix F	Near Trp^{164}	15.87	25.52	6.52	–	**Val^{163}, Trp^{164}**
T184M	Proximal	β-Sheet	Near Mn^{2+} site	13.03	8.62	21.86	Ala^{174}, $\underline{Ile^{181}}$	Ala^{174}
Q202L	Proximal	β-Sheet	Buried	17.14	22.9	15.85	Ile^{199}, $\underline{Ala^{235}}$, 2×($\underline{Glu^{304}}$)	Ile^{199}, Glu^{304}
D213A	Proximal	Coil	Haem channel	20.25	20.31	29.46	–	–
G330R	C-terminus	Coil	Surface	18.09	8.57	27.07	–	**Val^{328}**

*Underlined residues indicate those involved in bonds interrupted after mutation; residues in bold indicate those involved in newly formed bonds after mutation.

Received 5 July 2011/7 October 2011; accepted 7 October 2011
Published as BJ Immediate Publication 7 October 2011, doi:10.1042/BJ20111199